NASA TM X-3250

NASA TECHNICAL MEMORANDUM

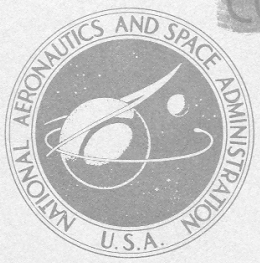

NASA TM X-3250

FLIGHT-DETERMINED LIFT AND DRAG CHARACTERISTICS OF AN F-8 AIRPLANE MODIFIED WITH A SUPERCRITICAL WING WITH COMPARISONS TO WIND-TUNNEL RESULTS

Jon S. Pyle and Louis L. Steers

Flight Research Center
Edwards, Calif. 93523

NATIONAL AERONAUTICS AND SPACE ADMINISTRATION • WASHINGTON, D. C. • JUNE 1975

[redacted] UNCLASSIFIED

1. Report No.	2. Government Accession No.	3. Recipient's Catalog No.
NASA TM X-3250		

4. Title and Subtitle	5. Report Date
FLIGHT-DETERMINED LIFT AND DRAG CHARACTERISTICS OF AN F-8 AIRPLANE MODIFIED WITH A SUPERCRITICAL WING WITH COMPARISONS TO WIND-TUNNEL RESULTS (U)	June 1975
	6. Performing Organization Code
7. Author(s)	8. Performing Organization Report No.
Jon S. Pyle and Louis L. Steers	H-843
	10. Work Unit No.
9. Performing Organization Name and Address	766-73-61
NASA Flight Research Center P. O. Box 273 Edwards, California 93523	11. Contract or Grant No.
	13. Type of Report and Period Covered
12. Sponsoring Agency Name and Address	Technical Memorandum
National Aeronautics and Space Administration Washington, D.C. 20546	14. Sponsoring Agency Code

15. Supplementary Notes

16. Abstract

Flight measurements obtained with a TF-8A airplane modified with a supercritical wing are presented for altitudes from 7.6 kilometers (25,000 feet) to 13.7 kilometers (45,000 feet), Mach numbers from 0.6 to 1.2, and Reynolds numbers from 0.8×10^7 to 2.3×10^7. Flight results for the airplane with and without area-rule fuselage fairings are compared. The techniques used to determine the lift and drag characteristics of the airplane are discussed. Flight data are compared with wind-tunnel model results, where applicable.

17. Key Words (Suggested by Author(s))	18. Distribution Statement
Supercritical wing Flight lift and drag characteristics Flight-to-wind-tunnel comparisons	U.S. Government and Contractors only STAR Category 02

19. Security Classif. (of this report)	20. Security Classif. (of this page)	21. No. of Pages	22. Price
[redacted]	Unclassified	87	

'NATIONAL SECURITY INFORMATION'
Unauthorized Disclosure Subject to Criminal Sanctions

[redacted]

[redacted]

UNCLASSIFIED

FLIGHT-DETERMINED LIFT AND DRAG CHARACTERISTICS OF AN F-8 AIRPLANE MODIFIED WITH A SUPERCRITICAL WING WITH COMPARISONS TO WIND-TUNNEL RESULTS

Jon S. Pyle and Louis L. Steers
Flight Research Center

INTRODUCTION

A supercritical airfoil has been developed to increase the drag-rise Mach number for a given lift coefficient or to increase the lift coefficient for separation onset at a given Mach number (refs. 1 to 4). Wind-tunnel studies were conducted to determine the feasibility of applying a supercritical airfoil to a transport configuration. As a result of the wind-tunnel studies, a wind-tunnel and flight test program was initiated to verify the advantages of the supercritical wing with an existing airplane.

A TF-8A airplane was chosen as a test-bed to demonstrate the supercritical wing concept. The supercritical wing was adapted to this airplane's fuselage; henceforth, in this paper, this airplane is referred to as the F-8 supercritical wing airplane. Wind-tunnel studies (refs. 5 and 6) were conducted to adapt the new wing to the test vehicle and to determine the vehicle's performance, stability, and control characteristics. Flight tests were conducted to verify the characteristics predicted by the wind-tunnel studies and to determine the value of the supercritical wing concept in a flight environment. Reference 7 is a preliminary report of the results obtained during these proof-of-concept flight tests.

These first flight tests were conducted with a nonoptimum area distribution. The area distribution of the basic configuration was not particularly well suited to speeds near Mach 1; therefore, the distribution was improved by adding area-rule fairings to the fuselage. This paper presents the lift and drag characteristics determined in flight for both configurations (with and without the area-rule fuselage fairings) and compares the flight and wind-tunnel data for each case.

The flight results are for altitudes from 7.6 kilometers (25,000 feet) to 13.7 kilometers (45,000 feet) and for Mach numbers from 0.6 to 1.2.

SYMBOLS

Physical quantities in this report are given in the International System of Units (SI) and parenthetically in U.S. Customary Units. Measurements were taken in SI Units. Details concerning the use of SI Units, together with physical quantities and conversion factors, are given in reference 8.

A_c	cross-sectional area of the airplane perpendicular to the airplane's longitudinal axis, m^2 (ft^2)
A_d	cross-sectional area of the inlet duct at the engine compressor face, m^2 (ft^2)
A_e	area of the exit nozzle, m^2 (ft^2)
A_i	cross-sectional area of the inlet duct at the inlet, m^2 (ft^2)
a_n	airplane acceleration measured normal to the airplane's longitudinal axis, g
a_x	airplane acceleration measured along the airplane's longitudinal axis, g
C_D	total airplane drag coefficient
C_{D_B}	drag coefficient measured on the base of the airplane
C_{D_β}	drag coefficient measured over the boattailed portion of the engine shroud
$\Delta C_D/\Delta M$	ratio of the change in total airplane drag coefficient to the change in free stream Mach number
C_f	thrust coefficient obtained from ground calibration
C_L	lift coefficient
C_{L_α}	lift-curve slope, ratio of lift coefficient to airplane angle of attack, per deg
$\Delta C_L/\Delta C_D$	slope of the lift coefficient versus the drag coefficient

C_m	pitching moment coefficient
C_N	normal force coefficient
C_p	static-pressure coefficient obtained normal to surface of vehicle
C_{p_β}	static-pressure coefficient measured over the boattailed portion of the engine shroud
C_X	axial force coefficient
D	total airplane drag, kN (lb)
F_G	gross engine thrust, kN (lb)
F_N	net engine thrust, kN (lb)
F_R	ram drag of inlet air, kN (lb)
h	altitude, m (ft)
$\dot{h}$	rate of change in altitude, m/sec (ft/sec)
L	total airplane lift
M	free stream Mach number
M_d	Mach number measured in the inlet duct at the engine compressor face
m	mass flow of the free stream air, (kN-sec)/m ((lb-sec)/ft)
m_d	mass flow of the air through the duct, (kN-sec)/m ((lb-sec)/ft)
P	free stream static pressure, kN/m^2 (lb/ft^2)
P_d	static pressure measured in the inlet duct at the engine compressor face, kN/m^2 (lb/ft^2)
P_{t_d}	total pressure measured in the inlet duct at the engine compressor face, kN/m^2 (lb/ft^2)
P_{t_e}	total pressure measured at the engine exit nozzle, kN/m^2 (lb/ft^2)
q	dynamic pressure, kN/m^2 (lb/ft^2)

R	Reynolds number
S	planform area of the supercritical wing, m^2 (ft^2)
T	free stream temperature, °K (°R)
T_d	temperature of the air in the inlet duct, °K (°R)
$\dot{V}$	rate of change in velocity, m/sec^2 (ft/sec^2)
W	airplane weight, kN (lb)
x/l	ratio of distance along the airplane's longitudinal axis to the total airplane length
α	angle of attack, deg
$\Delta\alpha$	correction to angle of attack for in-flight calibration, deg
$\Delta\alpha_B$	correction to angle of attack for nose-boom bending during normal acceleration, deg
δ_e	average deflection of horizontal stabilizers, deg
γ	ratio of specific heats
θ	circumferential location of boattail orifices on the aft portion of the airplane fuselage, deg

VEHICLE DESCRIPTION

Flight Vehicle

The TF-8A airplane provided the empennage, fuselage, and propulsion systems for the supercritical wing flight tests (figs. 1(a) and 1(b)). The TF-8A airplane is a single-place interceptor powered by a J57-P4 turbojet engine with afterburner capability. Air is supplied to the engine by means of a main duct through the fuselage. The duct inlet is approximately 0.79 meter (2.6 feet) behind the apex of the airplane's nose cone.

In its original configuration, the airplane had a variable incidence, high-mounted wing that was easy to replace with the supercritical wing. A three-view drawing of the F-8 supercritical wing airplane is presented in figure 1(c). The horizontal and vertical stabilizers were not changed for the test program.

The cross-sectional area distribution of the F-8 supercritical wing airplane is shown in figure 2. The distribution for the first flight tests (without area-rule

fuselage fairings) included the fiber glass wing-body juncture fairing (fig. 3(a)) and the vertical stabilizer fairings (fig. 3(b)). The machine-gun discharge ports were also enclosed by fairings (fig. 3(c)).

After the first flight tests were completed, fairings were added to the sides of the fuselage just in front of and behind the wing (figs. 3(d) and 3(e)). These fairings were intended to reduce wave losses near the speed of sound and thus increase the airplane's drag-rise Mach number.

Several small protuberances on the fuselage contributed to the total drag of the airplane and were, therefore, simulated in the wind-tunnel model (fig. 3(f), ref. 9).

Wing.—The planform area of the supercritical wing, based on the extension of the leading and trailing edges of the wing to the fuselage centerline, is approximately 26 square meters (275 square feet). The wing is attached to the fuselage at an incidence angle of 1.5° at the root chord. It has an aspect ratio of 6.8 and a sweep angle of 42.24° along the quarter chord. The streamwise thickness-to-chord ratio varies from 11 percent at the wing-body juncture to 9 percent at the mean geometric chord; it is approximately 7 percent at the wingtip. Additional information concerning wing dimensions and structure is presented in references 9 and 10.

Vortex generators (fig. 3(g)) were installed at the 60-percent semispan on the bottom leading edge of the wing. These devices were used to improve the pitching moment characteristics of the test configuration at high angles of attack (ref. 11). Fairings (fig. 3(h)) were also added to the underside of each wing to cover the aileron hinges.

Aft fuselage.—The aft 14.7 percent of the fuselage (fig. 4) has a 7° boattail angle. The boattail area was instrumented with surface-pressure orifices to make comparisons between the flight and wind-tunnel boattail drag results possible.

The annular base area of the airplane (figs. 4 and 5(a)) was 0.645 square meter (6.94 square feet) with the afterburner off and 0.497 square meter (5.35 square feet) with the afterburner on. This area consisted of the cavity between the engine variable exit nozzle and the fuselage boattail shroud, which extended 1.37 meters (4.5 feet) in back of the aft fuselage firewall.

Wind-Tunnel Model

A sting-supported 0.087-scale model of the F-8 supercritical wing airplane was tested in the Langley 8-Foot Transonic Pressure Tunnel. The tests defined the aerodynamic characteristics and surface-static-pressure coefficients of the model with and without the area-rule fuselage fairings. Many of the airplane's protuberances, such as the air data probe, antennas, light, camera fairing plate, vortex generators, machine gun discharge port fairings, and aileron hinge fairings, were scaled to the model size and included in the test configuration. Pressure orifices were installed on the boattail of the model as close as possible to the locations of those on the flight vehicle, and pressure measurements were obtained for all tests. A more complete description of the model and test facility is given in reference 9.

INSTRUMENTATION

Flight

Flight lift and drag were calculated from measurements made with onboard instrumentation. All measurements were recorded on board with magnetic tape and telemetered to a ground station by a pulse code modulation system. The procedures and equations used to determine the angle of attack, thrust, and drag from the flight test measurements are presented in the appendix.

Air data probe.—Standard NACA flow direction sensors (ref. 12) and a Mach-number-compensated pitot-static probe designed for this configuration were mounted on the nose boom (ref. 13). The impact-pressure and compensated static-pressure orifices were 2.09 meters (6.85 feet) and 2.04 meters (6.68 feet) in front of the vehicle's nose, respectively. Angle of attack and angle of sideslip were measured by floating vanes that were 1.42 meters (4.67 feet) and 1.32 meters (4.32 feet) in front of the vehicle's nose, respectively. A temperature probe was mounted opposite the angle-of-attack vane to measure free stream total temperature.

In-flight calibrations of angle of attack indicated that some interference was occurring between the angle-of-sideslip and angle-of-attack vanes at Mach numbers near 1.0. The interference was eliminated by removing the sideslip vane and shaft. All flight results presented in this paper were obtained after the angle-of-sideslip vane and shaft were removed.

Lift and drag.—An accelerometer package that contained two longitudinal accelerometers (±0.25g and ±1.0g), two normal accelerometers (-4g to 1g and -3g to 6g), one transverse accelerometer (±1g), and a three-axis gyro was mounted on the main centerline keel beam 9.6 meters (31.5 feet) aft of the fuselage nose. The outputs of the ±0.25g longitudinal accelerometer and the -3g to 6g normal accelerometer were filtered to exclude frequencies greater than 10 cycles per second and corrected to the airplane center of gravity, zero angular velocity, and zero angular acceleration. The resulting accelerations were used to calculate the normal and axial forces exerted on the airplane. The total weight of the airplane at any time during a flight was calculated from recordings of fuel quantity and preflight gross weight.

Thrust.—The momentum of the air in the inlet as it entered the engine compressor face was calculated from measurements of total and static pressure obtained with rakes and static orifices (figs. 5(b) and 5(c)). The total-pressure measurement at the engine compressor face was obtained with five radial rakes, each of which contained five manifolded pressure probes. The pressure measurements from each rake (fig. 5(b)) were averaged to obtain the cross-sectional total pressure at the compressor face. In the same way, the static-pressure orifices around the pump housing of the engine (fig. 5 (c)) and the engine duct were averaged to obtain the ambient pressure at the compressor face. All momentum losses in front of the compressor face were considered to be part of the drag of the fuselage.

The momentum of the air leaving the engine was measured by an air-cooled pitot probe mounted in the engine exhaust (figs. 5(a) and 5(d)). This measurement

procedure has been verified in experiments with a similar jet engine mounted in a high-performance airplane (refs. 14 and 15). The cooling air for the exhaust probe was obtained from the last stage of the engine compressor.

Boattail and base pressures.—A series of surface-pressure orifices was installed at circumferential stations of 8°, 46°, 135°, and 180° along the right half of the boattailed portion of the fuselage (fig. 4). The orifices were in six rings around the fuselage that were between 94.7 percent and 99.6 percent of the fuselage length.

Base pressures were measured at four circumferential locations (0°, 90°, 180°, and 270°) inside the base cavity of the fuselage. Both the boattail and base pressure measurements were obtained with a scanivalve transducer in a rear section of the fuselage.

Pressures along area-rule fuselage fairings.—The airplane area-rule fuselage fairings were not originally equipped with the orifices and internal tubing necessary for pressure measurements. Therefore, flexible vinyl tubing with static orifices (figs. 6(a) to 6(c)) was attached to the airplane's area-rule fuselage fairings in such a way that flight pressure measurements could be compared with existing wind-tunnel data. The tubing was faired to the fuselage surface with an aircraft sealer. Orifices were cut in the tubing at approximately the same locations as used in the wind-tunnel tests. Some orifice tubes were installed off the centerline of the fairing to determine the effects of attitude and cross-flow interference. Pressure measurements were obtained with existing internal instrumentation.

Wind Tunnel

Force and moment data (ref. 9) were obtained in the Langley 8-Foot Transonic Pressure Tunnel with a strain-gage balance mounted in the fuselage cavity of a 0.087-scale model of the airplane. Pressures at the orifices along the area-rule fuselage fairings and on the boattailed portion of the fuselage were measured with a differential-pressure scanning-valve mounted in the model's nose section. Static pressures were measured in the balance chamber and on the base plane of the model to determine the base drag. When the wind-tunnel results were analyzed, the base pressures were adjusted to ambient conditions. Thus, all the drag results presented in reference 9 represent wind-tunnel model drag without base drag.

TEST CONDITIONS

Flight

The flight data presented in this paper were obtained from long-period accelerating turns and quasi-stabilized, constant altitude runs at altitudes of 7.6 kilometers (25,000 feet), 10.7 kilometers (35,000 feet), and 13.7 kilometers (45,000 feet). The Mach number range of the tests varied from 0.6 to 1.2. Reynolds number, based on the wing mean geometric chord, varied from 0.8×10^7 to 2.3×10^7. The center-of-gravity position for the tests was approximately 25 percent of the wing mean geometric chord.

Wind Tunnel

Wind-tunnel measurements (ref. 9) were made over a Mach number range from 0.25 to 1.0. Angle of attack varied from -5° to 12°; angle of sideslip was 0°. The Reynolds numbers of the wind-tunnel tests varied from 1.8×10^6 to 3.0×10^6 based on the wing mean geometric chord of the wind-tunnel model.

The internal flow through the model was constricted by the sting support used to mount the model in the Langley 8-Foot Transonic Wind Tunnel. Therefore, to simulate the internal mass flow ratios that were expected with the airplane, two exit ducts were used during the wind-tunnel model tests. Both ducts were wholly contained within the scaled base lines of the airplane. Wind-tunnel data for the two ducts were compared to obtain an adjustment for the increase in internal drag due to the sting support (ref. 6). This adjustment was made to all the wind-tunnel results used in this paper.

FLIGHT DATA ACCURACY

The parameters that contributed to random error in the flight results are listed in the following table. The table is based on data obtained for a Mach number of 0.97, a lift coefficient of 0.4, and an altitude of 13.7 kilometers (45,000 feet).

Parameter	Error in measurement	Error in C_L, percent	Error in C_D, percent
Weight	±4.4 kN (±100 lb)	0.4	---
Dynamic pressure	±0.06 kN/m^2 (±1.3 lb/ft^2)	0.6	0.6
Net thrust	±0.36 kN (±80 lb)	---	3.8
Normal acceleration	±0.01g	1.0	0.6
Longitudinal acceleration	±0.001g	---	1.2
Angle of attack	±0.25°	---	5.0
Root-sum-squared error		1.3	6.4

To minimize bias errors, calibrations were obtained for the instrumentation both in the laboratory and on the airplane. In addition, preflight and postflight weighings and instrument zeros were recorded for each flight. To further reduce bias errors, the flight results presented were obtained during several flights at the same Mach number and altitude conditions. Therefore the random error in fairings of the flight results is believed to be minimal.

CORRECTIONS TO WIND-TUNNEL DATA

Several corrections were made to the wind-tunnel drag results that, although not discussed in reference 9, are normally applied to wind-tunnel data to make comparisons with flight results realistic. For example, the corrections applied to the wind-tunnel data for a Mach number of 0.90 and a lift coefficient of 0.4 were as follows:

Corrections (measured and calculated)	Area-rule fuselage fairings	
	Off	On
Transition	0.0015	0.0015
Internal drag	-0.00485	-0.0047
Reynolds number	-0.0045	-0.0045
Roughness	0.0015	0.0015
Total	-0.00635	-0.0062

The correction for transition refers to the correction that was made to the wind-tunnel data to account for differences in skin friction between the wind-tunnel and airplane wing. Transition strips were placed on the wind-tunnel wing at the 5-percent or 31-percent chord, depending on the Mach number of the wind-tunnel test (ref. 9), to simulate the trailing-edge boundary-layer thickness expected in flight. The transition strips tripped the boundary layer and caused the flow to be turbulent over the remainder of the wing. Wind-tunnel oil flow studies verified that the flow was laminar in front of the strip. The airplane wing is considered to be fully turbulent in flight, so the laminar flow regions on the wind-tunnel model wing were corrected to turbulent skin friction drag conditions.

The correction for the model support interference (internal drag) is discussed in TEST CONDITIONS.

The wind-tunnel force data were corrected to the flight Reynolds numbers by subtracting the increments of drag that resulted from the difference between the skin friction drag of the model and that of the full-scale vehicle. In addition, an estimated roughness drag increment (ref. 16) was added to the wind-tunnel results to correct for the difference in smoothness between the model and the full-scale airplane.

These corrections were applied to all wind-tunnel trimmed drag data presented in this paper. The drag measurements made on the model in the wind tunnel were obtained at three horizontal stabilizer deflections (-5°, -2.5°, and 0°). The drag measurements were corrected to trim conditions by interpolating the drag polars between the wind-tunnel data points adjusted to the trim condition ($C_m = 0$) at each stabilizer setting.

RESULTS AND DISCUSSION

Flight Results

The lift curves and drag polars obtained from flight measurements for the airplane without area-rule fuselage fairings are presented in figures 7 to 9. Data are presented for various Mach numbers and altitudes.

The effect of altitude (including Reynolds number) on the drag results is shown in figure 10. The drag coefficient is presented as a function of Mach number for a constant lift coefficient near the design trim condition ($C_L = 0.4$). The drag-rise Mach number ($\Delta C_D/\Delta M = 0.1$) varies from 0.95 at the lowest altitude to 0.97 at the highest altitude. There is some drag creep (a slight gradient in drag before the drag-rise Mach number) in the data for an altitude of 13.7 kilometers (45,000 feet). The agreement of the data for altitudes of 7.6 kilometers (25,000 feet) and 10.7 kilometers (35,000 feet) is close.

The effect of altitude on the lift of the airplane is presented in figure 11. At the higher lift coefficients and the intermediate Mach numbers (0.9 and 0.97), there are some changes in the lift-curve slopes for the various altitudes. These changes are believed to be due to variations in local angle of attack on the outboard portion of the wing. This change in local angle of attack at the various altitudes is due to the flexibility of the wing (ref. 7).

The lift curves and drag polars obtained after the area-rule fuselage fairings were added to the airplane are presented in figure 12. The data were obtained at an altitude of 10.7 kilometers (35,000 feet), and Reynolds number varied from 1.3×10^7 to 1.8×10^7.

Faired flight results with and without the area-rule fuselage fairings are compared in figure 13. The data in figure 13(a) indicate that the fairings had little effect on the flight lift curves. In addition, the lift-curve slopes for all Mach numbers are similar.

The area-rule fuselage fairings were added to the airplane to reduce its absolute drag at Mach numbers between 0.95 and 1.0, increasing the drag-rise Mach number. However, the drag polars presented in figure 13(b) show that the addition of the area-rule fuselage fairings resulted in slightly higher drag values at most Mach numbers.

Comparison of Flight and Wind-Tunnel Results

Mass flow.—The airflow through the inlet of the F-8 supercritical wing model was measured during the wind-tunnel tests (ref. 9). These wind-tunnel results are compared with flight results in figure 14. The data for configurations with and without the area-rule fuselage fairings are compared for a Mach number range from 0.8 to 0.99.

The data are for a constant angle of attack of 4°, which is near the trim condition. The flight measurements of airflow in the duct were acquired by using the following equation from reference 14:

$$\frac{m_d}{m} = \frac{P_d M_d A_d \sqrt{T}}{PMA_i \sqrt{T_d}} \sqrt{\frac{1 + 0.2M^2}{1 + 0.2M_d^2}}$$

There is a noticeable difference between the flight data with and without the area-rule fuselage fairings. The fairings near the duct inlet may have interfered with the airflow into the duct. This difference in mass flow ratios is not apparent in the wind-tunnel data. With the exception of the data for $M = 0.99$, the wind-tunnel mass flow ratios are higher than those measured in flight.

Base drag.—Figure 15 compares the base drag coefficients measured in flight and in the wind tunnel. Both sets of test data were obtained with and without the area-rule fuselage fairings. The significant discrepancy between the flight and wind-tunnel results is probably due to the presence of the wind-tunnel support sting, which was attached to the model through its base area. This problem is common to all studies that use sting-mounted models (ref. 17). To make the comparisons of flight and wind-tunnel drag data in this investigation meaningful, base drag was removed from all the drag results.

Drag polars.—The data presented in figure 16 compare the wind-tunnel and flight drag polars (without base drag) for configurations with and without the area-rule fuselage fairings. In general, the level of drag in flight is significantly higher than predicted by the wind-tunnel results for lift coefficients at or below the approximate trim condition ($C_L = 0.4$). Differences were expected between the flight and wind-tunnel results at other than the design cruise lift coefficient, because the wind-tunnel model wing was designed to give the proper twist and bending at the design cruise condition only. Even at the trim condition, however, there was a difference of as much as 10 percent at the lower Mach numbers and as much as 30 percent at $M = 0.99$.

As might be expected from a wing designed to the trimmed condition, there is a noticeable difference between the flight and wind-tunnel drag polar curvatures. This difference in drag due to lift is emphasized by the comparison of the drag polars for the low and high lift coefficients in figure 16. The slopes of the flight drag polars ($\Delta C_L/\Delta C_D$) for a lift coefficient of 0.4 are from 5 percent to 25 percent lower than those obtained from the wind-tunnel data.

The inability of the wind tunnel to predict the flight values of drag due to lift at Mach numbers from 0.85 to 1.0 is attributed to wall interference on the model. The model wing was altered ("tuned") during the testing at the design point to obtain the desired lift and drag characteristics. However, the real flow environment over the trailing edge of the wing was masked by the wave reflections from the wind-tunnel walls. Therefore, when the final wing configuration was scaled to the airplane, the resulting full-scale wing had excessive camber along the trailing edge.

Although the area-rule fuselage fairings had little effect on the wind-tunnel drag values at Mach numbers below 0.97, the drag level for the configuration with the fairings is lower than the drag level for the configuration without them at $M = 0.99$ (fig. 16). In the flight data, however, the drag level for the configuration with the fairings is equal to or higher than the drag level for the configuration without the fairings throughout the Mach number range shown.

Trim characteristics.—Another reason for the disagreement between the flight and wind-tunnel drag levels is that the model and airplane had to use different horizontal stabilizer deflections to maintain comparable lift coefficients (fig. 17). The wind-tunnel data indicate that the model required less stabilizer deflection to maintain a given lift coefficient than the airplane. If the wind-tunnel model horizontal stabilizer deflections are adjusted to the airplane deflections, the wind-tunnel drag coefficients at $C_L = 0.4$ increase. This adjustment, which would increase total model drag at $C_L = 0.4$ by 3 percent to 5 percent, would account for some of the difference in the drag levels in figure 16.

Lift curves.—There is little difference between the flight and wind-tunnel lift curves presented in figure 18.

The flight and wind-tunnel results in figure 19, which shows the variation of the lift-curve slopes with Mach number, also agree well.

Boattail drag.—The boattail drag results for the airplane and model (figs. 20 and 21) also explain some of the difference between the flight and wind-tunnel drag levels. Typical boattail pressure measurements are presented in figure 20 for configurations with and without the area-rule fuselage fairings. The pressure coefficients, which are for a Mach number of 0.9, are plotted at their percentage location along the fuselage at four circumferential rows. The wind-tunnel pressures are generally higher than the flight results.

The difference between the flight and wind-tunnel boattail pressures is more obvious if the results are converted to drag. Figure 21 compares flight and wind-tunnel boattail drag at Mach numbers from 0.90 to 1.00. The difference is due primarily to the presence of the sting in the base area of the model (ref. 17). Adjusting the wind-tunnel drag for $C_L = 0.4$ to account for the differences between the flight and wind-tunnel boattail results also tends to bring the drag polars closer together.

Figure 22 compares the flight and wind-tunnel surface pressures measured along the center of the area-rule fuselage fairings for Mach numbers from 0.8 to 0.98

for a lift coefficient of 0.4. With the exception of the measurements at the 24-percent locations, the flight and wind-tunnel pressure coefficients on the forward fairing agree well. The flight data for the sloping surface of the rear fairing (beyond x/l = 75 percent) are somewhat different from the wind-tunnel data, particularly at a Mach number of 0.98, where the flight pressures are significantly lower than the wind-tunnel pressures. It was not determined whether this difference in pressures was due to the different horizontal stabilizer positions during the flight and wind-tunnel tests, the influence of the support sting, or the effects of wall interference during the wind-tunnel tests.

Total drag.—The variation of the total trimmed drag minus the base drag of the airplane and the model is presented in figure 23 as a function of Mach number. The arrowheads on the curves indicate the drag-rise Mach number ($\Delta C_D/\Delta M$ = 0.1) of each configuration. The drag-rise Mach number measured in flight without area-rule fuselage fairings agreed within 0.01 Mach number of the drag-rise Mach number predicted by the wind-tunnel tests.

The wind-tunnel data (ref. 9) indicate that the drag-rise Mach number was 0.01 higher for the model with the area-rule fuselage fairings. The flight data, however, show that the area-rule fuselage fairings did not increase the drag-rise Mach number.

Up to a Mach number of 0.95, the drag level of both airplane configurations was approximately 15 percent to 20 percent higher than indicated by the corresponding wind-tunnel results. At these Mach number conditions a significant part of the difference between the flight and wind-tunnel drag was probably due to the effect of the sting on the aft portion of the model's fuselage.

CONCLUDING REMARKS

The lift and drag characteristics of a TF-8A airplane modified with a supercritical wing were determined in flight and compared with wind-tunnel results. The drag-rise Mach number measured in flight without the area-rule fuselage fairings agreed within 0.01 Mach number of the drag-rise Mach number predicted by the wind-tunnel tests. The addition of the area-rule fuselage fairings to the F-8 supercritical wing configuration did not increase the drag-rise Mach number of the airplane as had been predicted by the wind-tunnel results.

Significant differences were noted between the flight and wind-tunnel values for base and boattail drag. In addition, the drag-due-to-lift characteristics of the model were different from those of the airplane. In general, the level of drag in flight was higher than predicted by the wind-tunnel results for lift coefficients at or below the design trim condition.

Flight Research Center
National Aeronautics and Space Administration
Edwards, Calif., January 16, 1975

APPENDIX

FLIGHT DATA ANALYSIS

Angle of Attack

The upwash effects from the nose boom and the fuselage (ref. 18), the aerodynamic forces on the boom, and the effect of pitching velocity and acceleration on the angle-of-attack vanes were computed and corrections were applied to the data. A static calibration of the nose-boom and the fuselage bending with normal and pitching acceleration was obtained by loading the nose boom. The results of this calibration, which are presented in figure 24(a), were applied to the flight results.

An in-flight calibration of angle of attack was obtained by measuring the longitudinal acceleration of the airplane in steady-state trimmed flight (where the changes in velocity, $\dot{V}$, and altitude, $\ddot{h}$, are zero). If the steady-state trimmed flight conditions are maintained, the true angle of attack is equal to the arc sine of the measured longitudinal acceleration. Although zero values of $\dot{V}$ and $\ddot{h}$ were difficult to maintain with the F-8 supercritical wing configuration, the deviations from the trimmed condition were small and could be corrected to obtain an angle-of-attack calibration. Figure 24(b) presents the correction to the angle of attack with the variation in Mach number as obtained by the in-flight calibration. This correction was also assumed to be valid for the nonsteady-state flight results (angles of attack higher or lower than trim) since the angle-of-attack range of this study was small.

Thrust Determination

The thrust of the F-8 supercritical wing airplane was determined in flight by the difference between the inlet momentum and the exit momentum of the airflow through the jet engine. A complete discussion and derivation of the thrust equations is given in reference 14. The inlet momentum (ram drag) can be calculated by the following equation:

$$F_R = \gamma P_d A_d M M_d \sqrt{\frac{1 + 0.2 M_d^2}{1 + 0.2 M^2}} \tag{1}$$

The static pressure in the duct, P_d, was measured at the engine compressor face (see INSTRUMENTATION). The cross-sectional area of the duct, A_d, was measured at the engine compressor face, where the static-pressure and total-pressure measurements were obtained. The free stream Mach number, M, and the ratio of specific heats, γ, were determined from airspeed probe data. The Mach number in the duct, M_d, was calculated from the following equation:

$$M_d = 2.236 \left(\frac{P_d}{P_{t_d}} - 1 \right)^{\frac{1}{2}} \tag{2}$$

APPENDIX - Continued

The gross engine thrust or exit momentum, F_G, was determined from the measurement of the free stream static pressure, P; the area of the exit nozzle, A_e; the thrust coefficient of the engine mounted in the airplane (calibrated on a ground thrust stand), C_f; the ratio of specific heats, γ; and the measured total pressure of the exhaust, P_{t_e}. Gross thrust was determined from the following equation:

$$F_G = PA_eC_f 2\frac{\gamma}{\gamma - 1}\left[\left(\frac{P_{t_e}}{P}\right)^{(\gamma-1)/\gamma} - 1\right] \tag{3}$$

This equation is valid for exit pressure ratios, $\frac{P_{t_e}}{P}$, up to 1.851 with the afterburner off or 1.802 with the afterburner on. Below these values, the exit pressure ratio is considered to be subcritical and the flow is subsonic. When the exit pressures are critical and the pressure ratios exceed the values above, the equation becomes:

$$F_G = A_eC_f\left[\left(\frac{2}{\gamma + 1}\right)^{\gamma/(\gamma-1)}(\gamma + 1)P_{t_e} - P\right] \tag{4}$$

Several thrust stand calibrations were made of the engine mounted in the F-8 supercritical wing airplane to determine its thrust coefficient at ground level. The thrust levels were obtained for various exit pressure ratios and are extrapolated to flight altitude conditions in figure 25. Altitude chamber tests on an early version of the J57 engine indicated that a variation in thrust coefficient of less than 2 percent occurs at altitudes between 4750 meters (15,000 feet) and 15,250 meters (50,000 feet). Therefore, the ground thrust stand results were extrapolated to the flight exit pressure ratios on the basis of previous experience with this engine (ref. 15 and unpublished data).

The net thrust of the engine is the difference between the gross thrust calculated with equation (3) or (4) and the ram drag calculated with equation (1). Thus, net thrust can be calculated as follows:

$$F_N = F_G - F_R \tag{5}$$

Drag Determination

Once an airplane's net thrust has been determined, its lift and drag characteristics can be calculated by using measurements of longitudinal and normal acceleration.

APPENDIX - Concluded

The following equations were used to compute the normal and axial forces from these measurements:

$$C_N = \frac{Wa_n}{qS} \tag{6}$$

$$C_X = \frac{F_N - Wa_x}{qS} \tag{7}$$

The force coefficients are transposed into the body axis coordinates by transforming with the airplane angle of attack; thus, equations (6) and (7) become:

$$C_L = C_N \cos \alpha - C_X \sin \alpha \tag{8}$$

$$C_D = C_N \sin \alpha + C_X \cos \alpha \tag{9}$$

$$L = C_L qS \tag{10}$$

$$D = C_D qS \tag{11}$$

$$\frac{L}{D} = \frac{C_L}{C_D} \tag{12}$$

[redacted]

REFERENCES

1. Whitcomb, Richard T.; and Clark, Larry R.: An Airfoil Shape for Efficient Flight at Supercritical Mach Numbers. NASA TM X-1109, 1965.

2. Whitcomb, Richard T.; and Blackwell, James A., Jr.: Status of Research on a Supercritical Wing. Conference on Aircraft Aerodynamics, NASA SP-124, 1966, pp. 367-381.

3. Harris, Charles D.: Wind-Tunnel Investigation of Effects of Trailing-Edge Geometry on a NASA Supercritical Airfoil Section. NASA TM X-2336, 1971.

4. Harris, Charles D.; and Blackwell, James A., Jr.: Wind-Tunnel Investigation of Effects of Rear Upper Surface Modification on an NASA Supercritical Airfoil. NASA TM X-2454, 1972.

5. Harris, Charles D.: Wind-Tunnel Measurements of Aerodynamic Load Distribution on an NASA Supercritical-Wing Research Airplane Configuration. NASA TM X-2469, 1972.

6. Bartlett, Dennis W.; and Re, Richard J.: Wind-Tunnel Investigation of Basic Aerodynamic Characteristics of a Supercritical-Wing Research Airplane Configuration. NASA TM X-2470, 1972.

7. Supercritical Wing Technology - A Progress Report on Flight Evaluations. NASA SP-301, 1972.

8. Mechtly, E. A.: The International System of Units - Physical Constants and Conversion Factors. Second Revision. NASA SP-7012, 1973.

9. Bartlett, Dennis W.; and Harris, Charles D.: Aerodynamic Characteristics of an NASA Supercritical-Wing Research Airplane Model With and Without Fuselage Area-Rule Additions at Mach 0.25 and 1.00. NASA TM X-2633, 1972.

10. Harris, Charles D.; and Bartlett, Dennis W.: Tabulated Pressure Measurements on an NASA Supercritical-Wing Research Airplane Model With and Without Fuselage Area-Rule Additions at Mach 0.25 to 1.00. NASA TM X-2634, 1972.

11. Harris, Charles D.; and Bartlett, Dennis W.: Wind-Tunnel Investigation of Effects of Underwing Leading-Edge Vortex Generators on a Supercritical-Wing Research Airplane Configuration. NASA TM X-2471, 1972.

12. Richardson, Norman R.; and Pearson, Albin O.: Wind-Tunnel Calibrations of a Combined Pitot-Static Tube, Vane-Type Flow-Direction Transmitter, and Stagnation-Temperature Element at Mach Numbers from 0.60 to 2.87. NASA TN D-122, 1959.

13. Ritchie, Virgil S.: Several Methods for Aerodynamic Reduction of Static-Pressure Sensing Errors for Aircraft at Subsonic, Near-Sonic, and Low Supersonic Speeds. NASA TR R-18, 1959.

[redacted]

14. Beeler, De E.; Bellman, Donald R.; and Saltzman, Edwin J.: Flight Techniques for Determining Airplane Drag at High Mach Numbers. NACA TN 3821, 1956.

15. Saltzman, Edwin J.; Bellman, Donald R.; and Musialowski, Norman T.: Flight-Determined Transonic Lift and Drag Characteristics of the YF-102 Airplane With Two Wing Configurations. NACA RM H56E08, 1956.

16. Horton, Elmer A.; and Tetervin, Neal: Measured Surface Defects on Typical Transonic Airplanes and Analysis of Their Drag Contribution. NASA TN D-1024, 1962.

17. Lee, George; and Summers, James L.: Effects of Sting-Support Interference on the Drag of an Ogive-Cylinder Body With and Without a Boattail at 0.6 to 1.4 Mach Number. NACA RM A57I09, 1957.

18. Yaggy, Paul F.: A Method for Predicting the Upwash Angles Induced at the Propeller Plane of a Combination of Bodies With an Unswept Wing. NACA TN 2528, 1951.

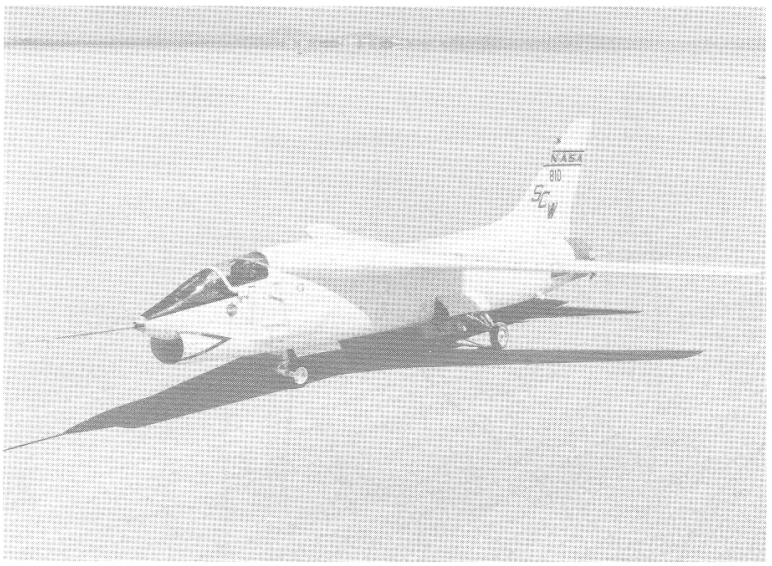

(a) Three-quarter front view. E-23122

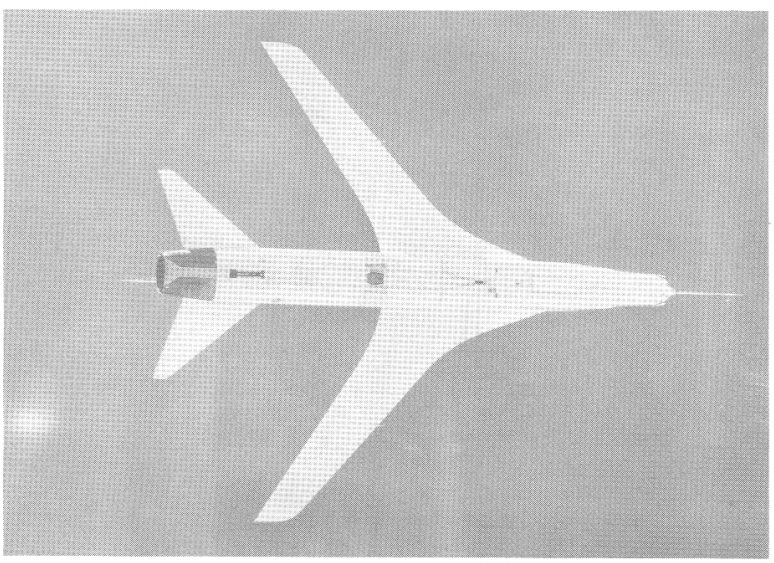

(b) Bottom view. E-22937

Figure 1. F-8 supercritical wing airplane.

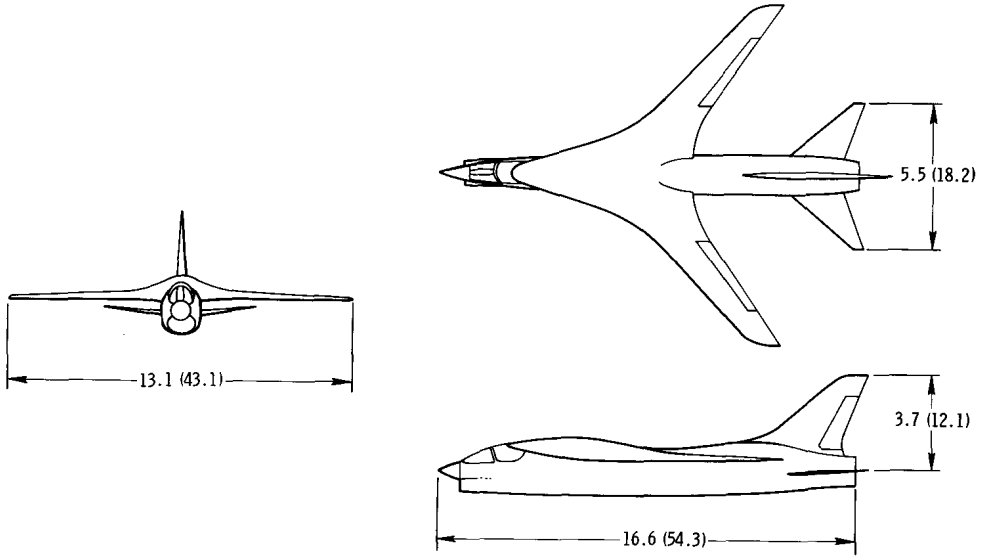

(c) Airplane dimensions (in meters (feet)).

Figure 1. Concluded.

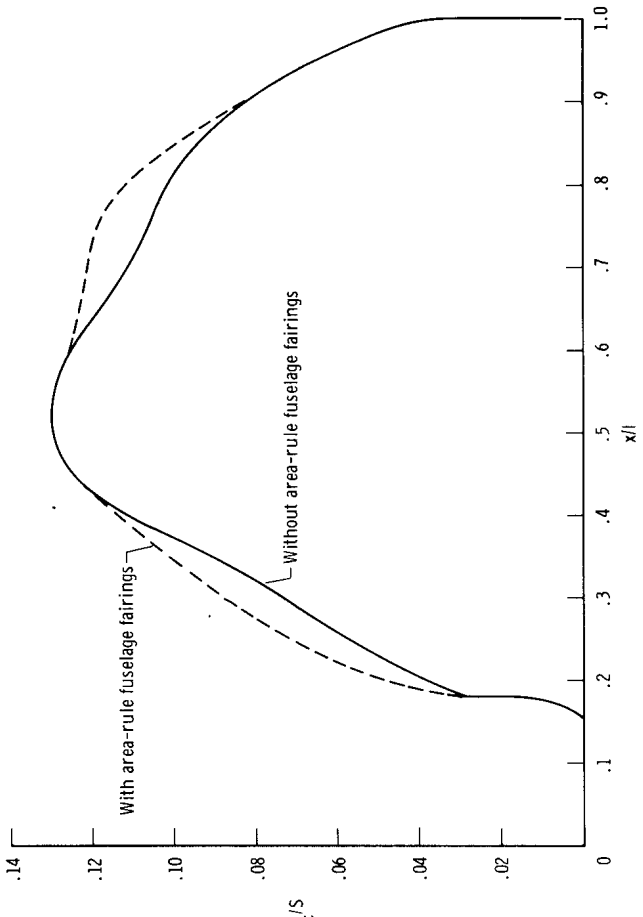

Figure 2. Airplane cross-sectional area distribution with and without area-rule fuselage fairings.

(a) Wing-body juncture. E-25080

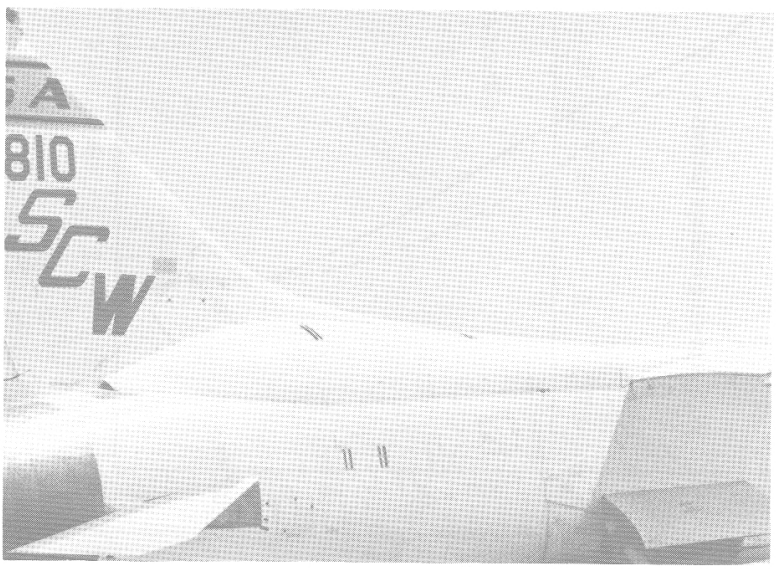

(b) Vertical stabilizer fairings. E-23111

Figure 3. Fairings and protuberances.

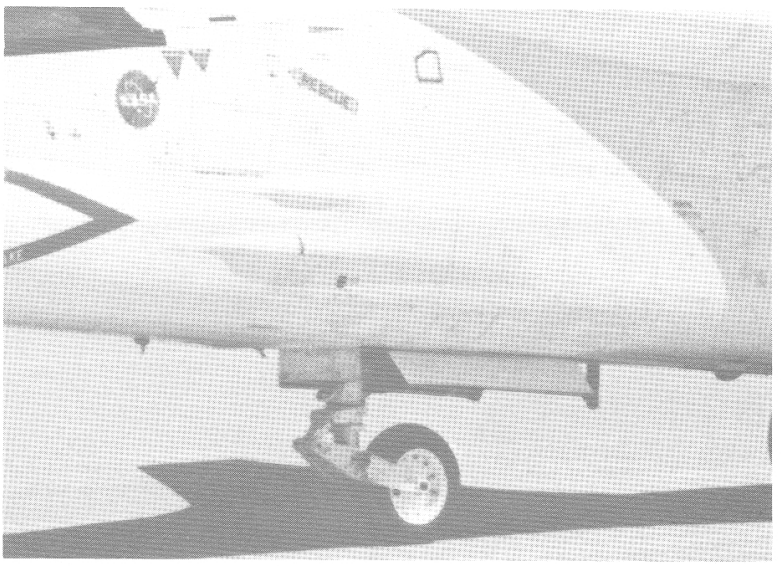

(c) Machine-gun fairings. E-23117

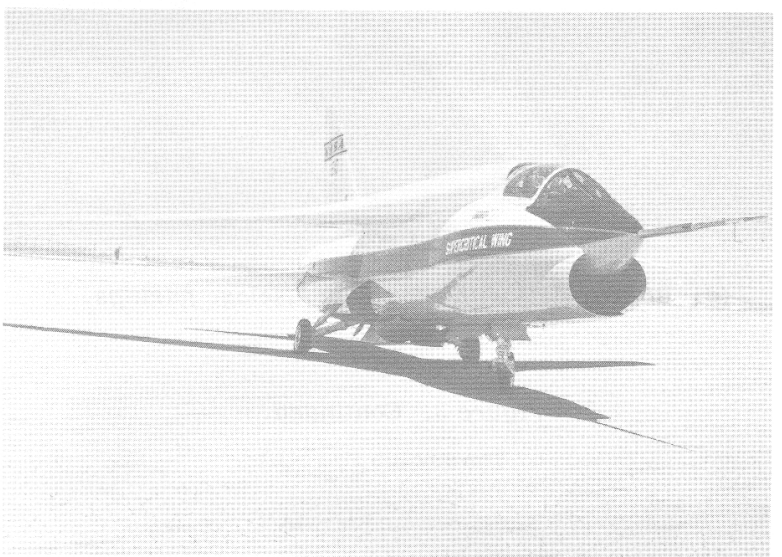

(d) Three-quarter front view with area-rule fuselage fairings. E-25087

Figure 3. Continued.

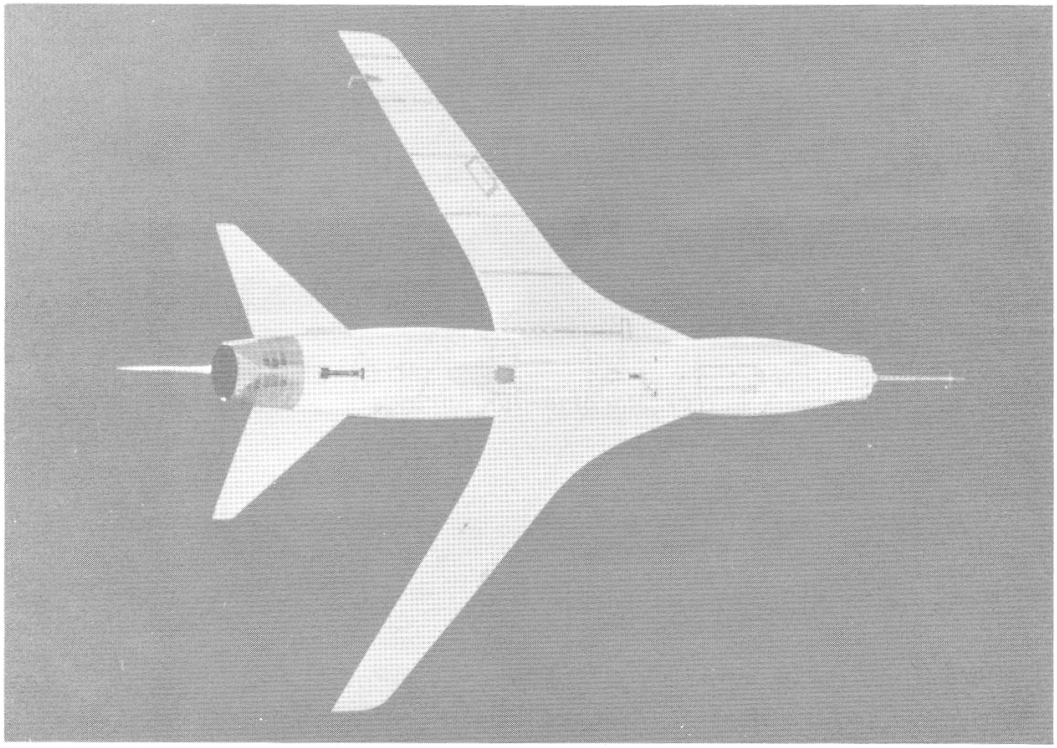

(e) Bottom view with area-rule fuselage fairings. *E-24893*

Figure 3. Continued.

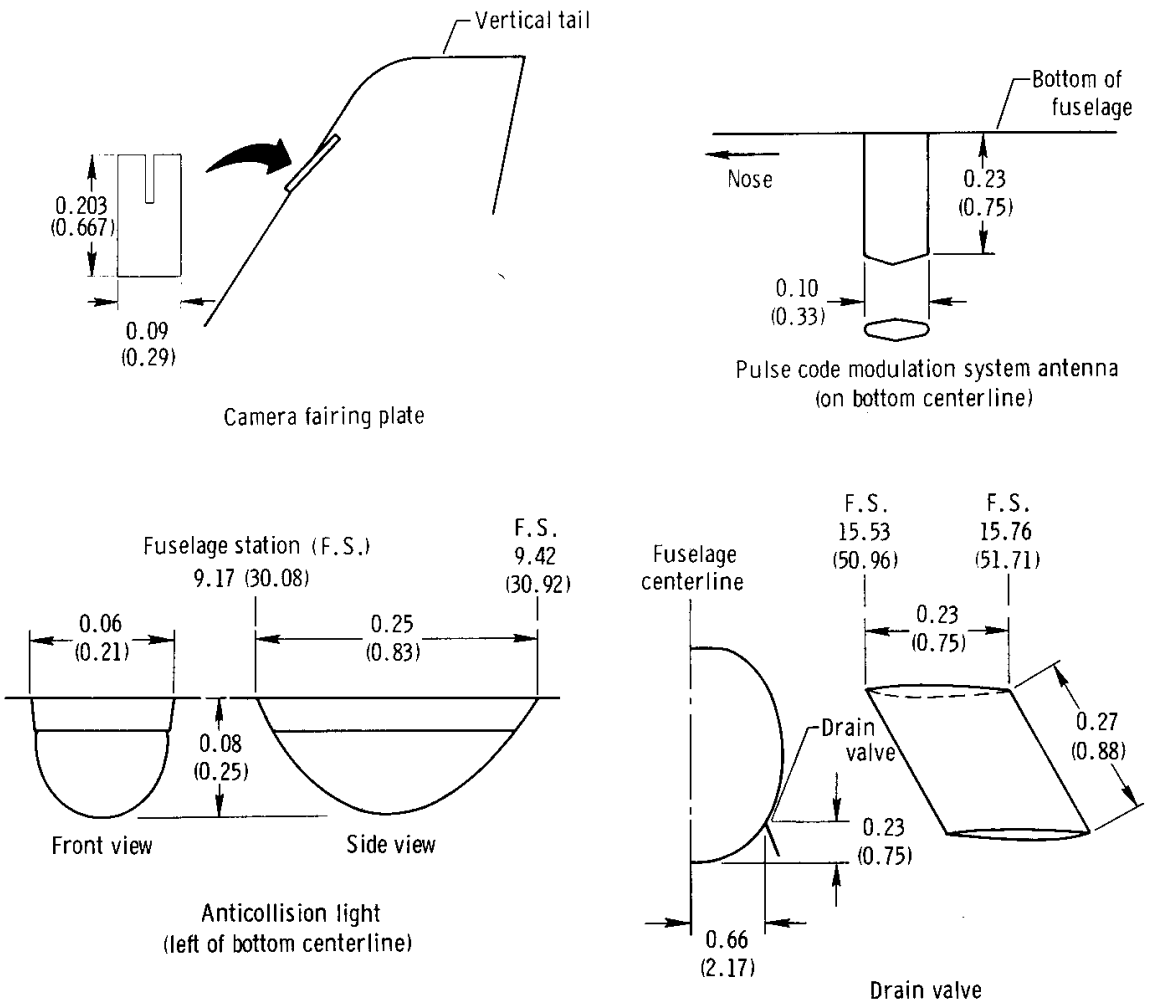

(f) Protuberances on airplane and wind-tunnel model. Dimensions are in meters (feet).

Figure 3. Continued.

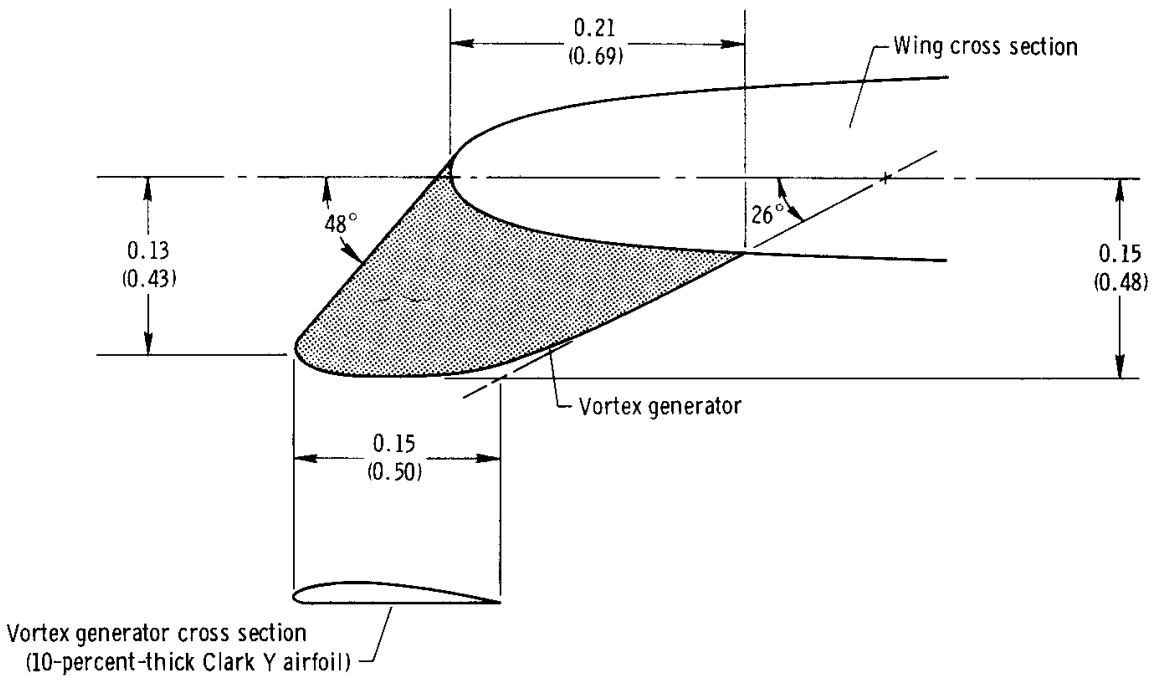

(g) Vortex generator on bottom leading edge of wing. Dimensions are in meters (feet).

Figure 3. Continued.

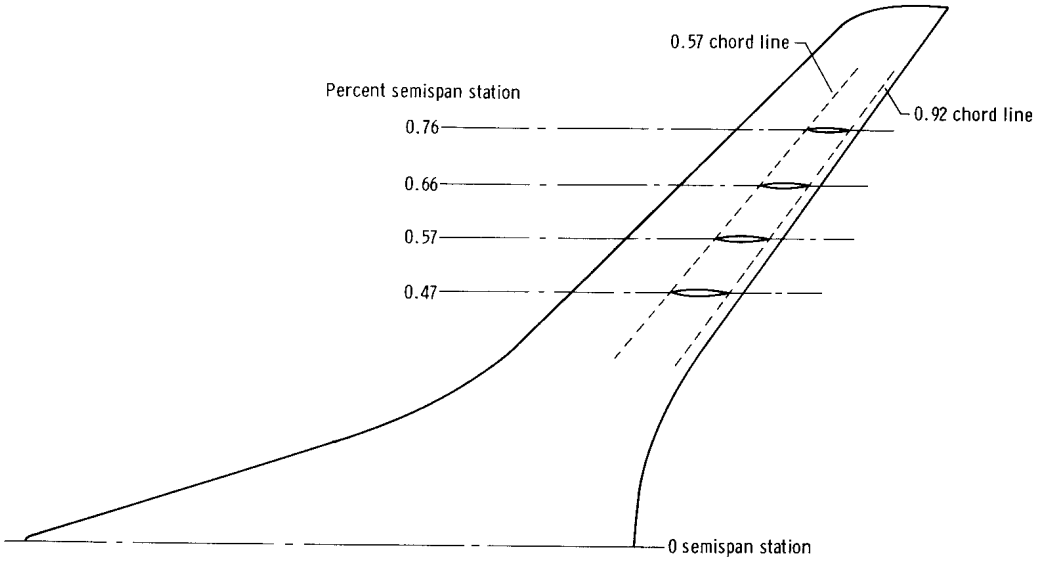

(h) Aileron hinge fairings on bottom of wing.

Figure 3. Concluded.

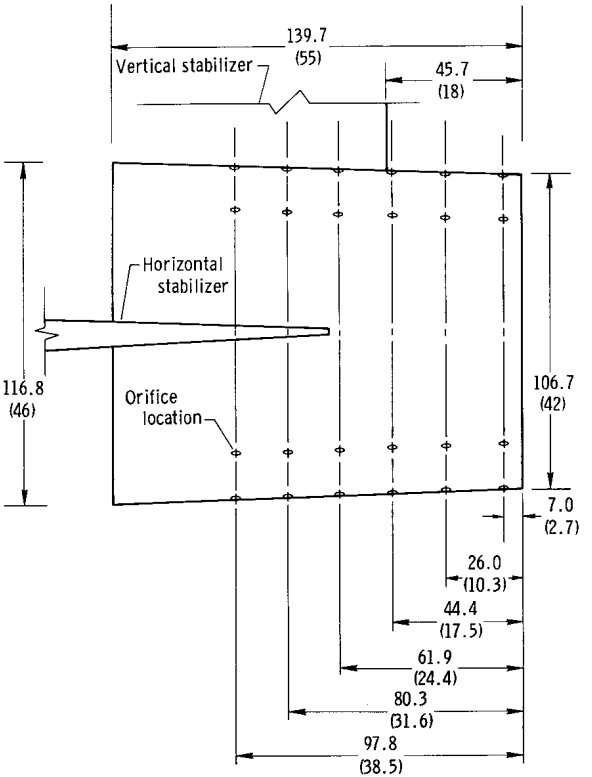

Side view

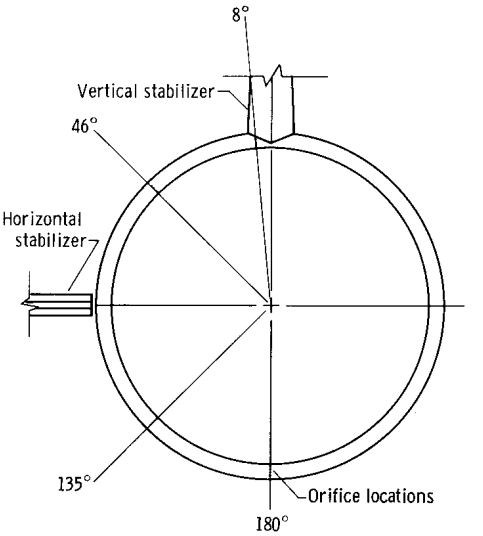

Rear view

Figure 4. Boattail pressure orifices. Dimensions are in centimeters (inches).

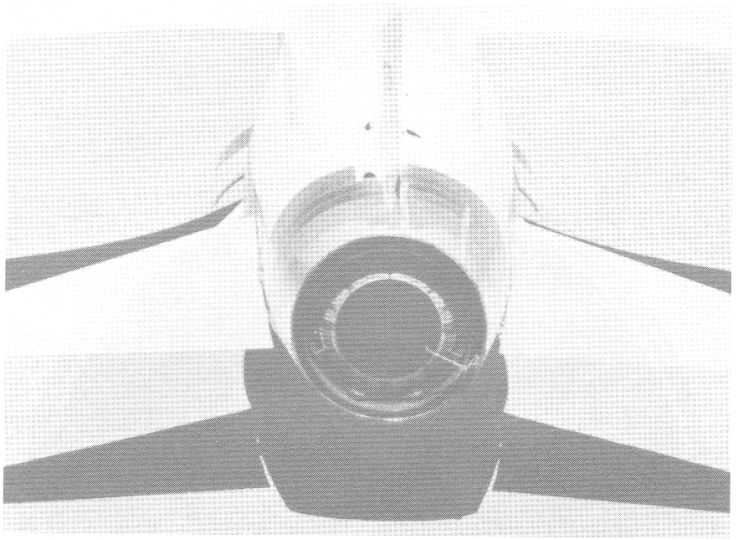

(a) Base area and variable ejector nozzle with tail pipe probe. E-25076

(b) Compressor face rake and static-pressure orifice. E-21770

Figure 5. Thrust instrumentation used to determine inlet and exit momentum of airflow through engine.

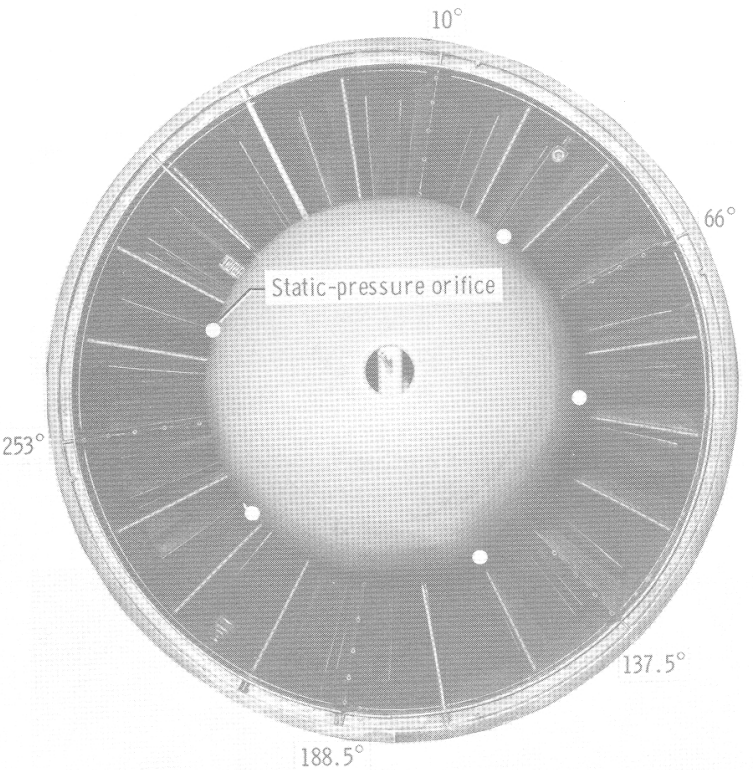

(c) Compressor face rakes and static-pressure orifices. E-21766

Figure 5. Continued.

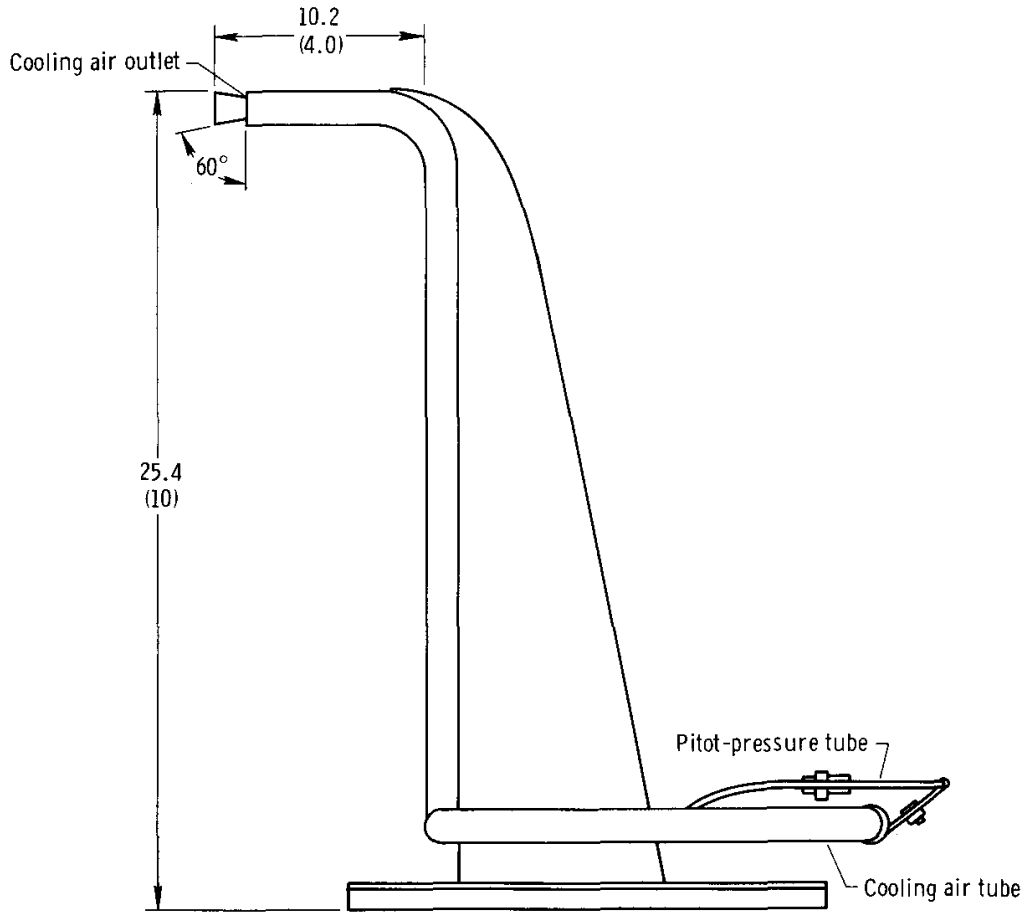

(d) Exit nozzle pitot probe. Dimensions are in centimeters (inches).

Figure 5. Concluded.

(a) Orifices on forward and aft area-rule fuselage fairings.

Figure 6. Location of vinyl tubing with static-pressure orifices on airplane fuselage.

(b) Orifices on forward area-rule fuselage fairings. E-25813

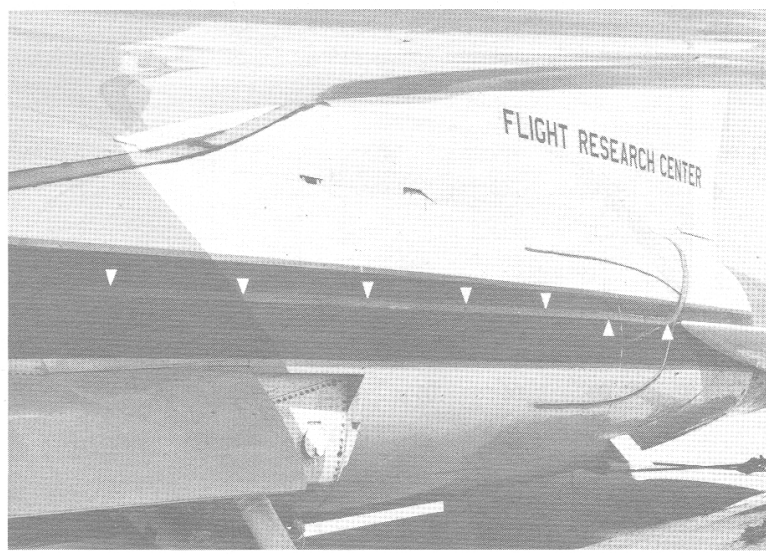

(c) Orifices on aft area-rule fuselage fairings. E-25815

Figure 6. Concluded.

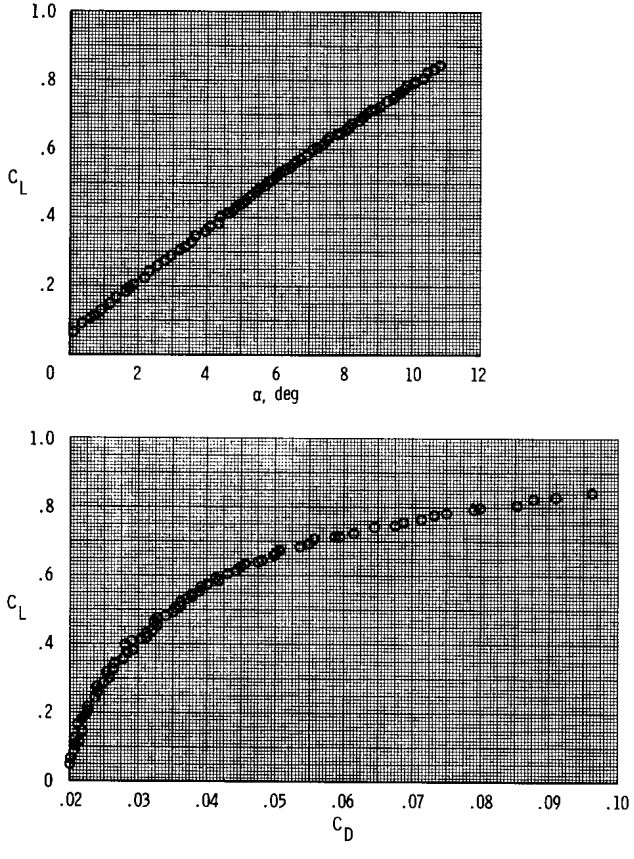

(a) $M = 0.6$, $R = 1.4 \times 10^7$.

Figure 7. Airplane lift and drag characteristics at an altitude of 7.6 kilometers (25,000 feet).

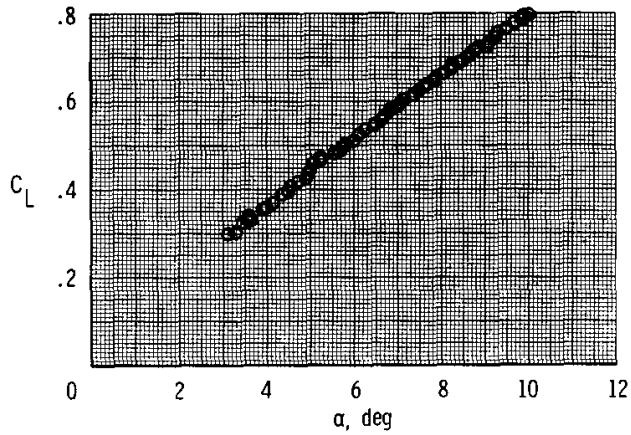

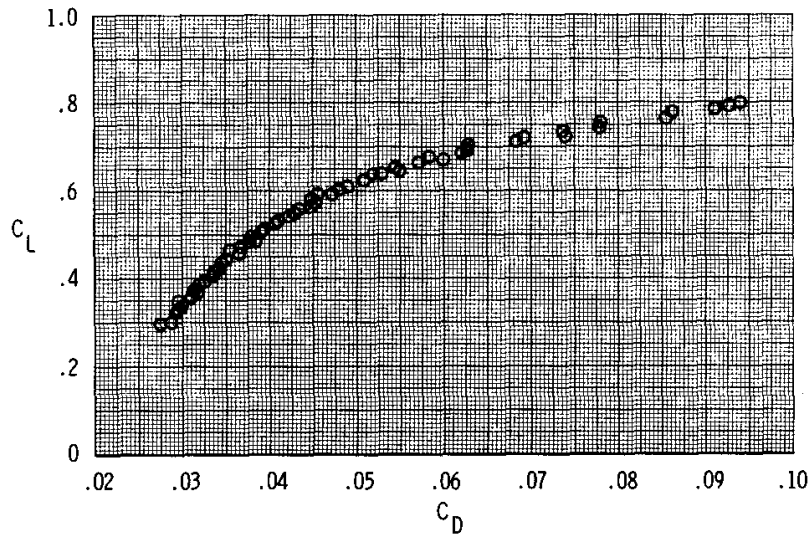

(b) $M = 0.7$, $R = 1.6 \times 10^7$.

Figure 7. Continued.

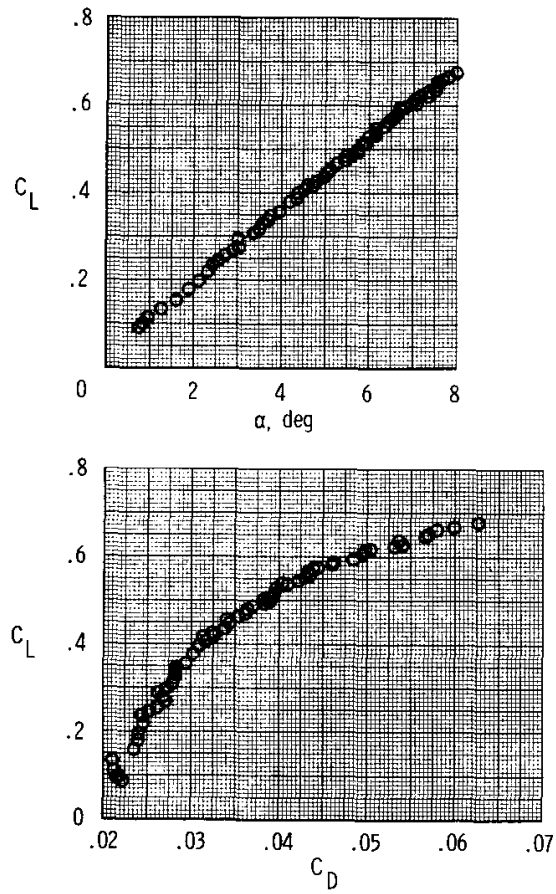

(c) $M = 0.8$, $R = 1.9 \times 10^7$.

Figure 7. Continued.

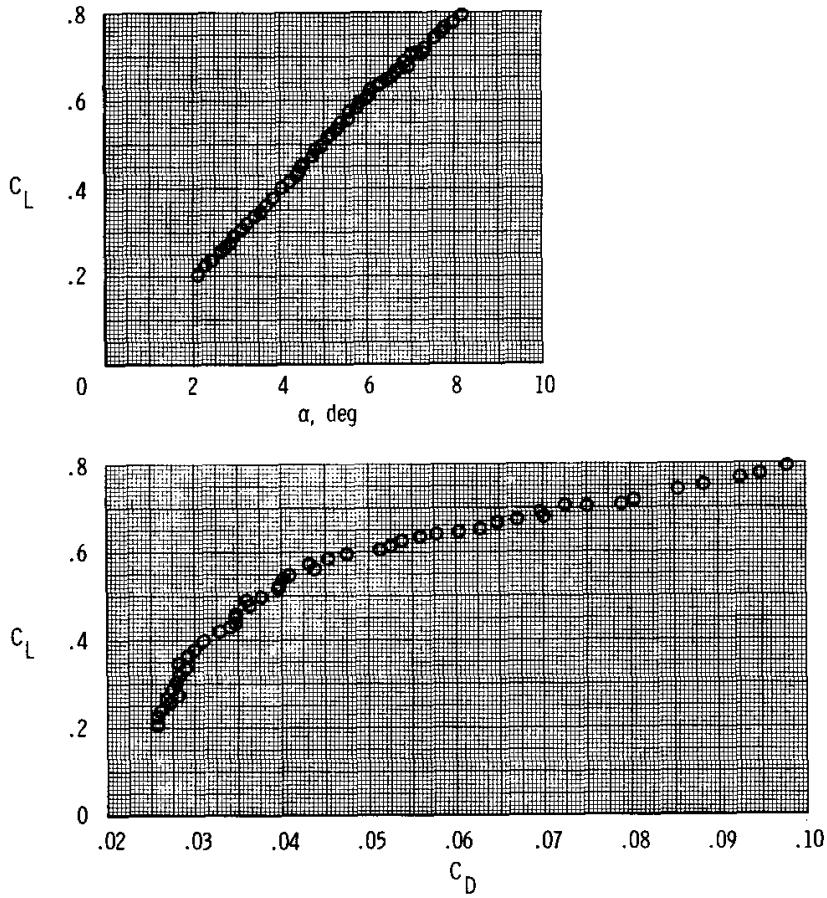

(d) $M = 0.9$, $R = 2.1 \times 10^7$.

Figure 7. Continued.

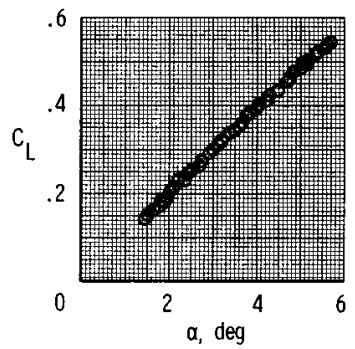

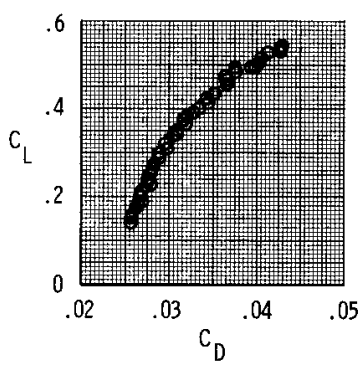

(e) $M = 0.95$, $R = 2.2 \times 10^7$.

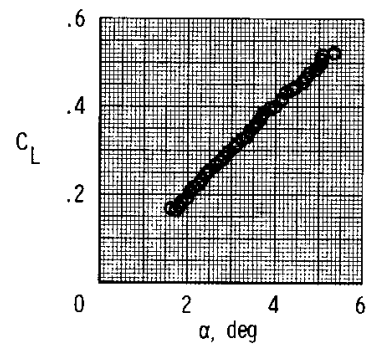

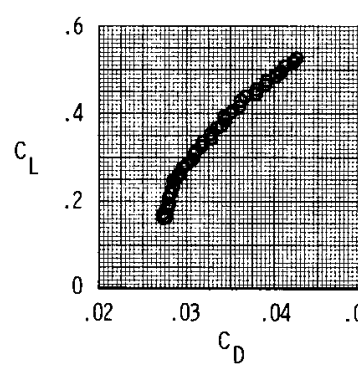

(f) $M = 0.96$, $R = 2.2 \times 10^7$.

Figure 7. Continued.

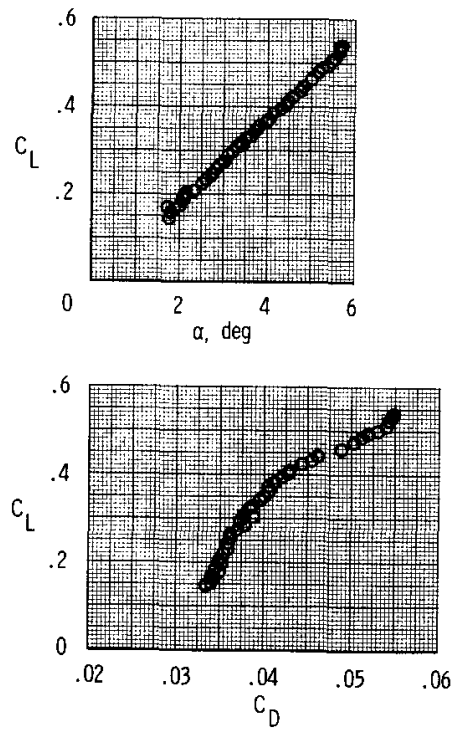

(g) $M = 0.98$, $R = 2.3 \times 10^7$.

Figure 7. Concluded.

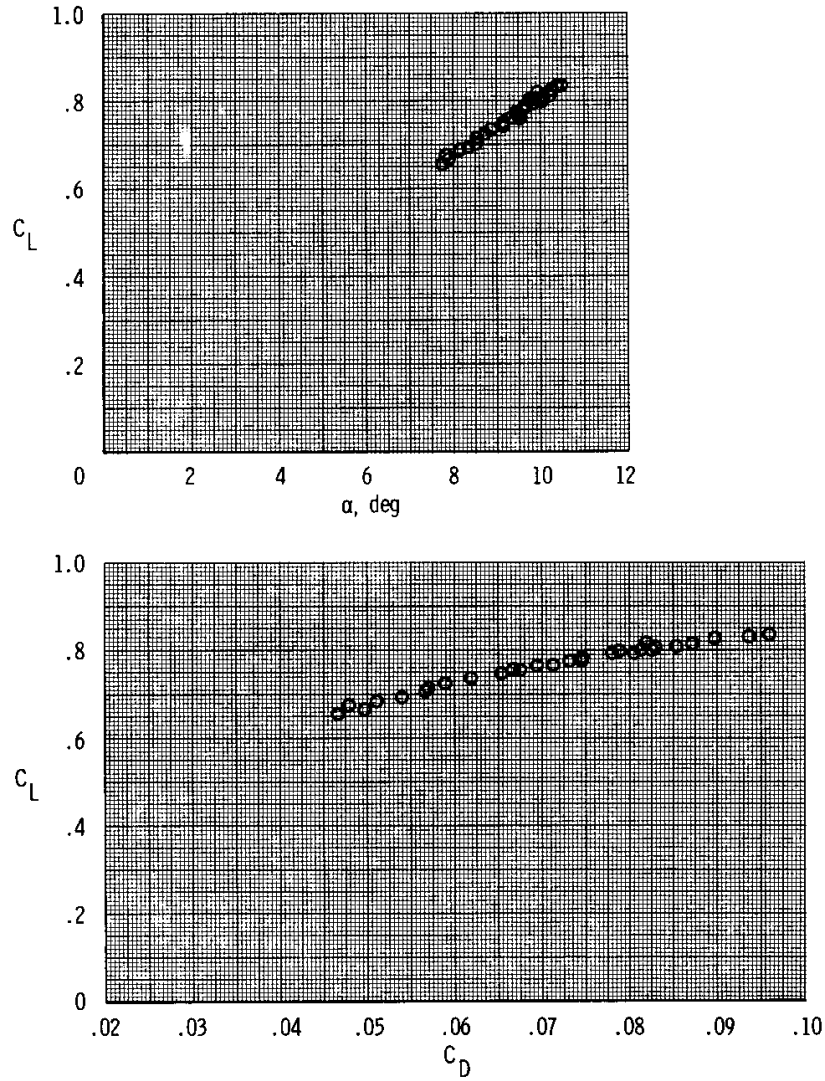

(a) $M = 0.6$, $R = 0.95 \times 10^7$.

Figure 8. Airplane lift and drag characteristics at an altitude of 10.7 kilometers (35,000 feet).

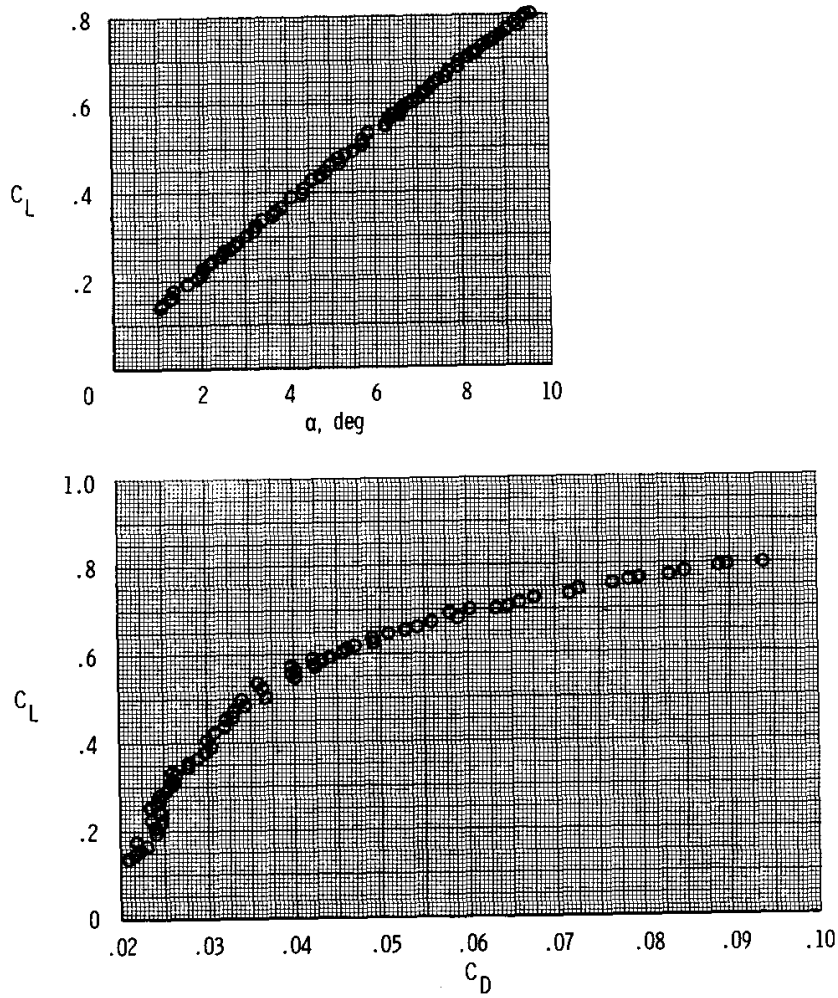

(b) $M = 0.7$, $R = 1.1 \times 10^7$.

Figure 8. Continued.

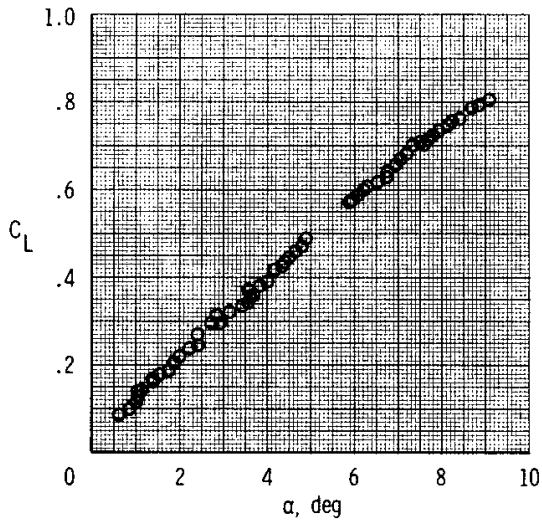

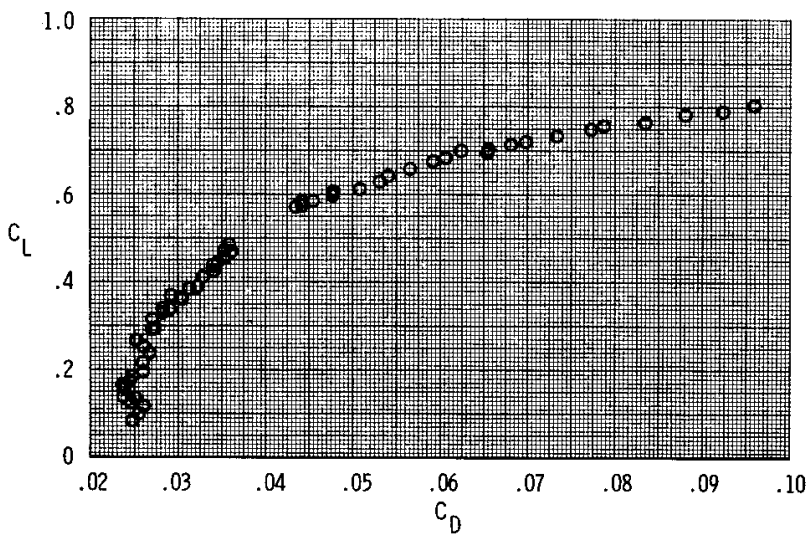

(c) $M = 0.8$, $R = 1.3 \times 10^7$.

Figure 8. Continued.

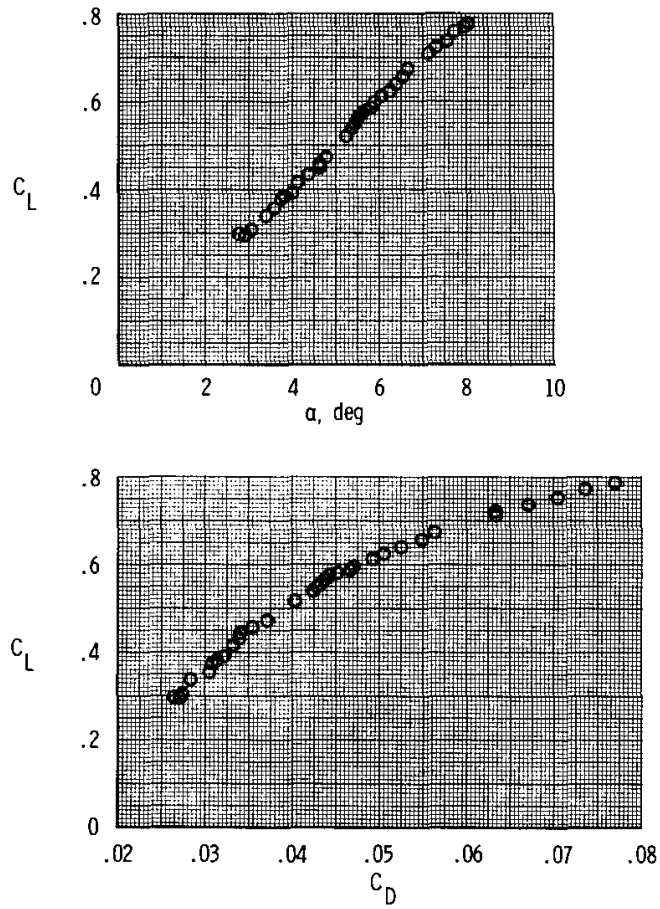

(d) $M = 0.9$, $R = 1.4 \times 10^7$.

Figure 8. Continued.

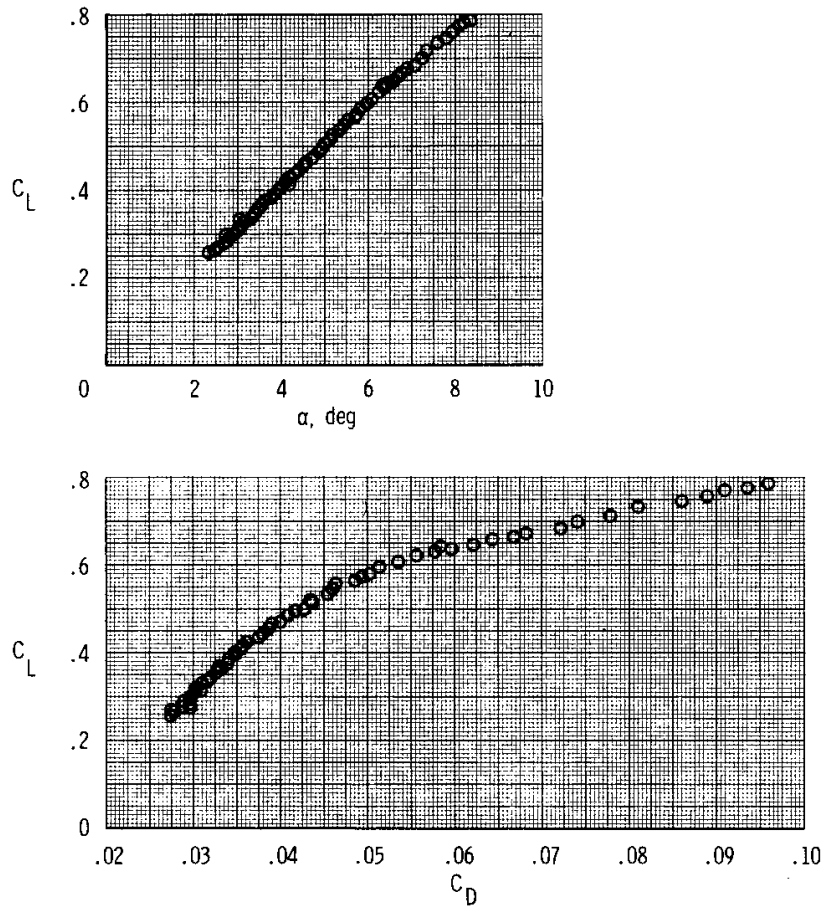

(e) $M = 0.95$, $R = 1.5 \times 10^7$.

Figure 8. Continued.

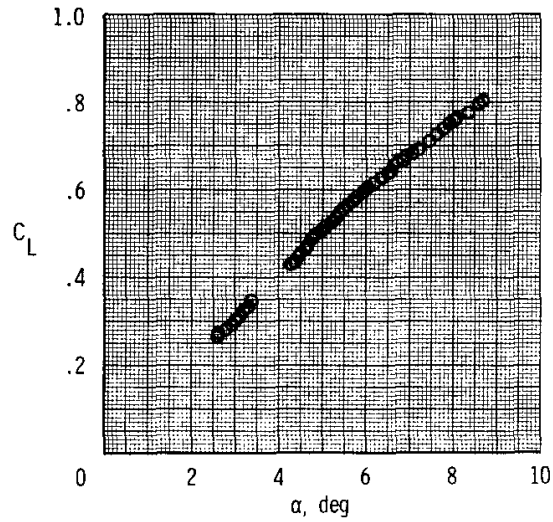

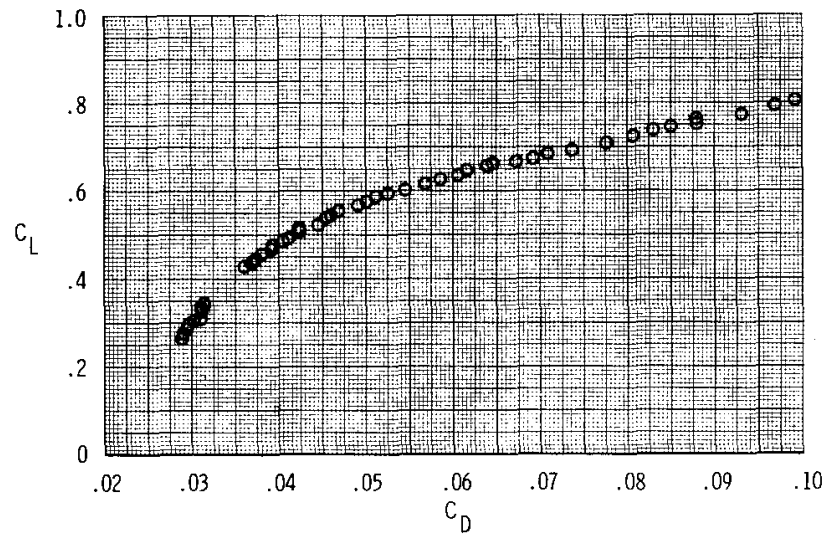

(f) $M = 0.96$, $R = 1.5 \times 10^7$.

Figure 8. Continued.

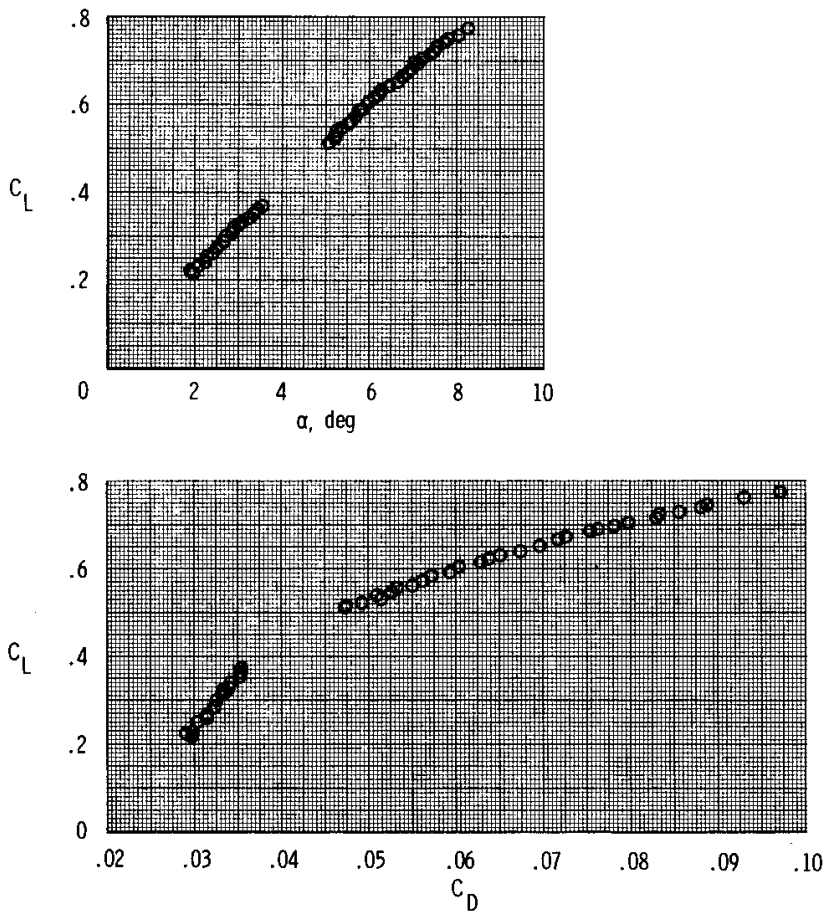

(g) $M = 0.97$, $R = 1.5 \times 10^7$.

Figure 8. Continued.

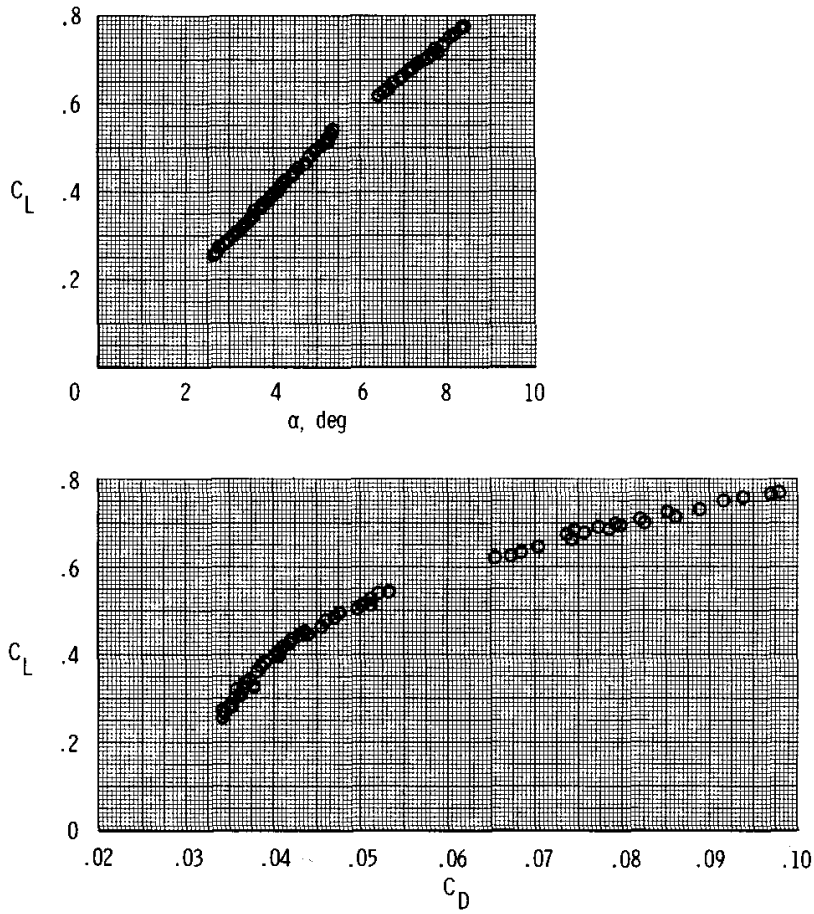

(h) $M = 0.98$, $R = 1.6 \times 10^7$.

Figure 8. Continued.

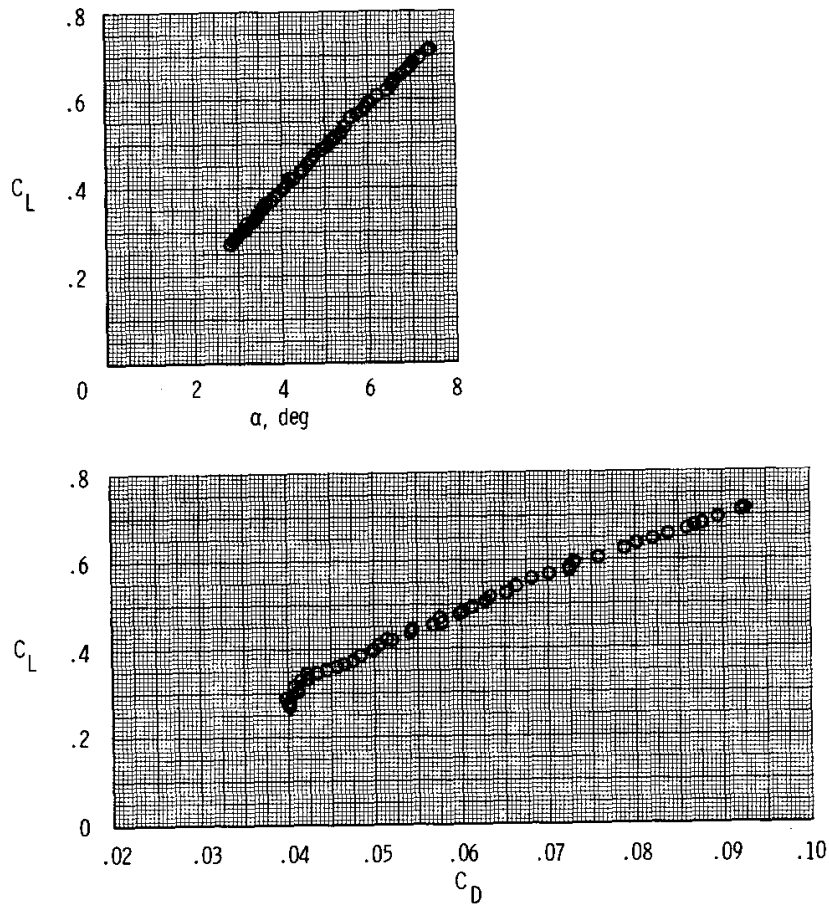

(i) $M = 0.99$, $R = 1.6 \times 10^7$.

Figure 8. Continued.

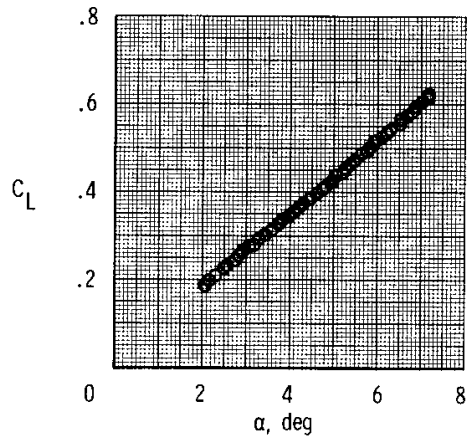

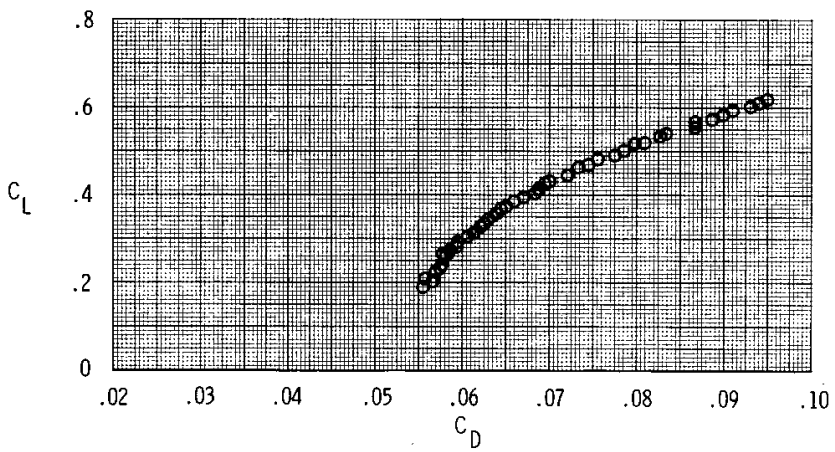

(j) $M = 1.1$, $R = 1.7 \times 10^7$.

Figure 8. Concluded.

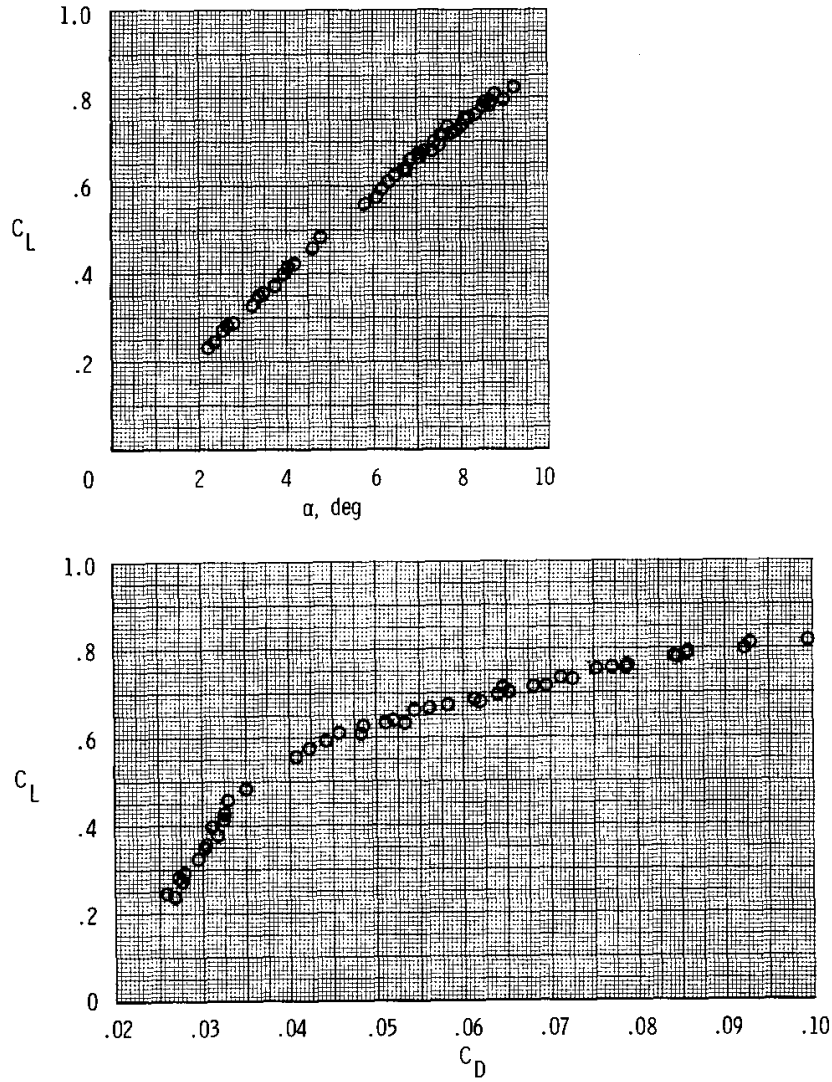

(a) $M = 0.8$, $R = 0.82 \times 10^7$.

Figure 9. Airplane lift and drag characteristics at an altitude of 13.7 kilometers (45,000 feet).

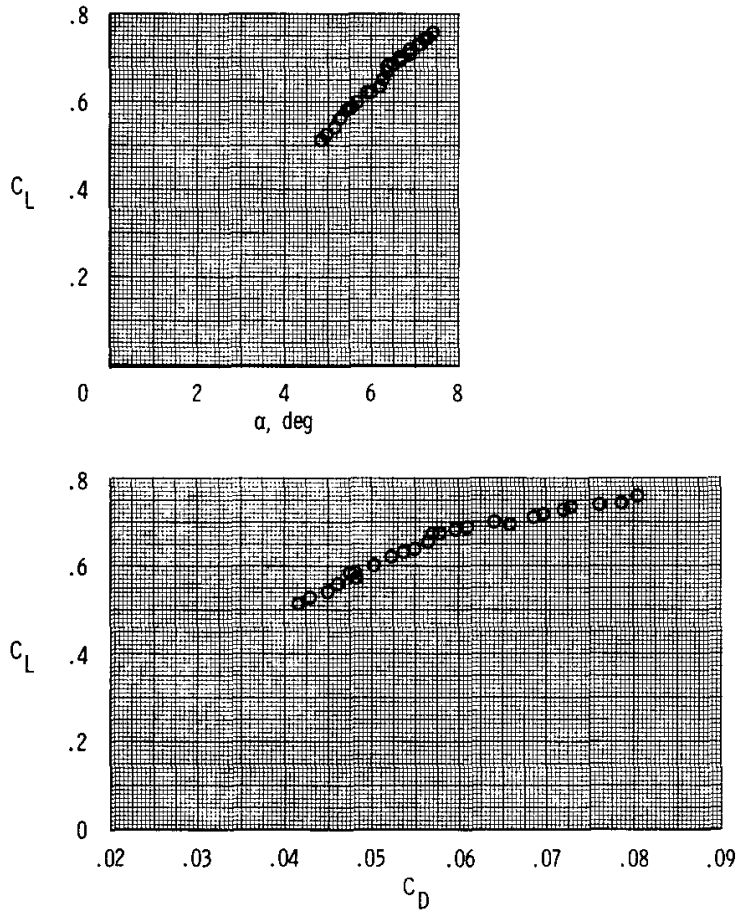

(b) $M = 0.9$, $R = 0.92 \times 10^7$.

Figure 9. Continued.

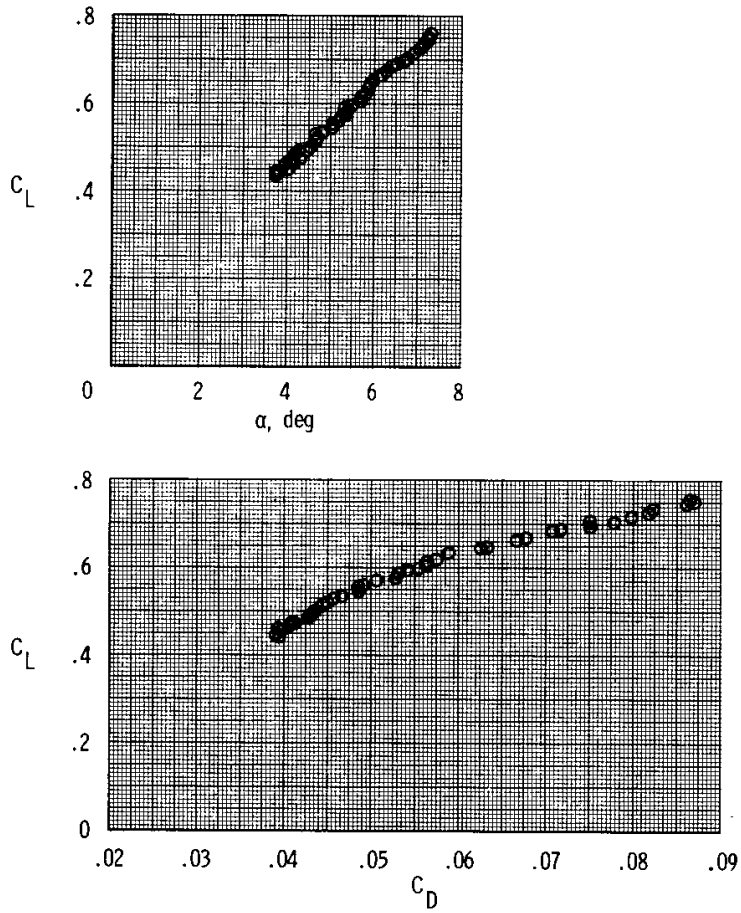

(c) $M = 0.95$, $R = 0.97 \times 10^7$.

Figure 9. Continued.

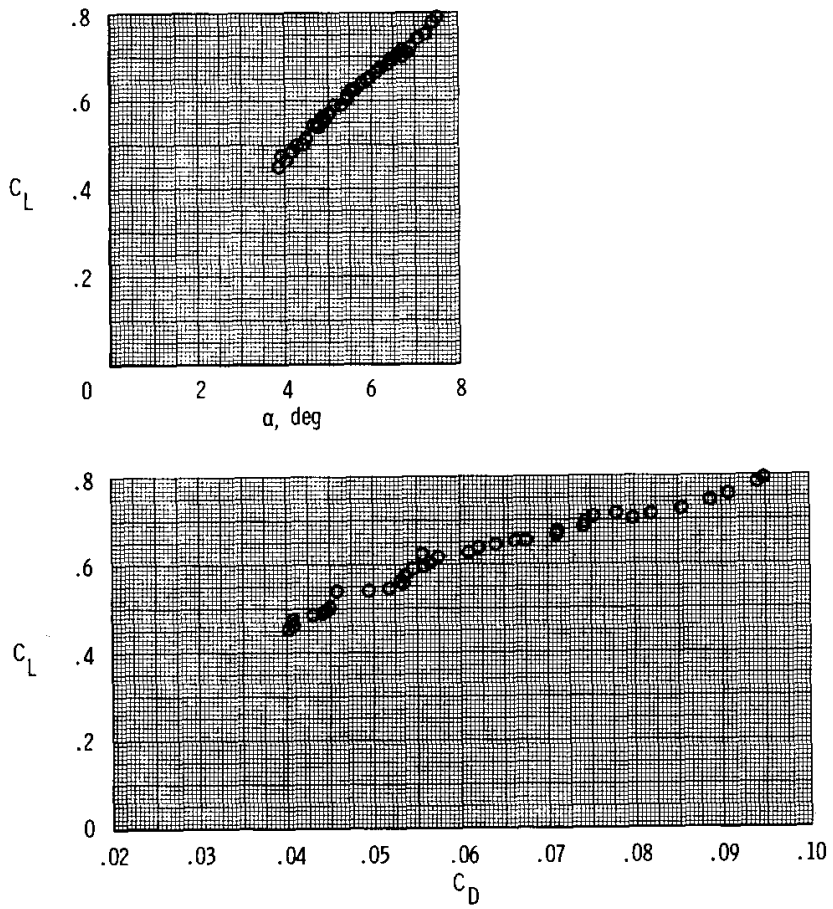

(d) $M = 0.97$, $R = 0.99 \times 10^7$.

Figure 9. Continued.

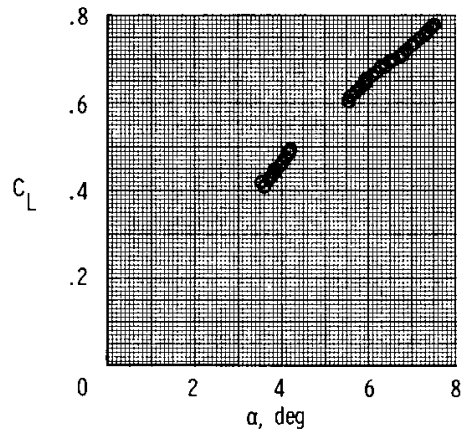

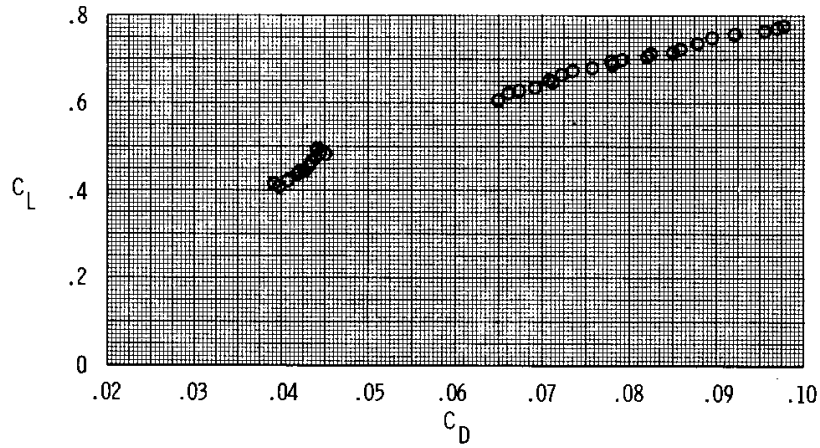

(e) $M = 0.98$, $R = 1.0 \times 10^7$.

Figure 9. Continued.

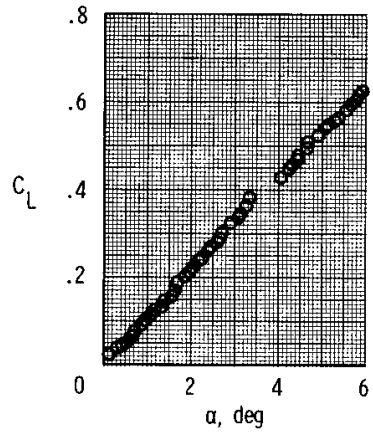

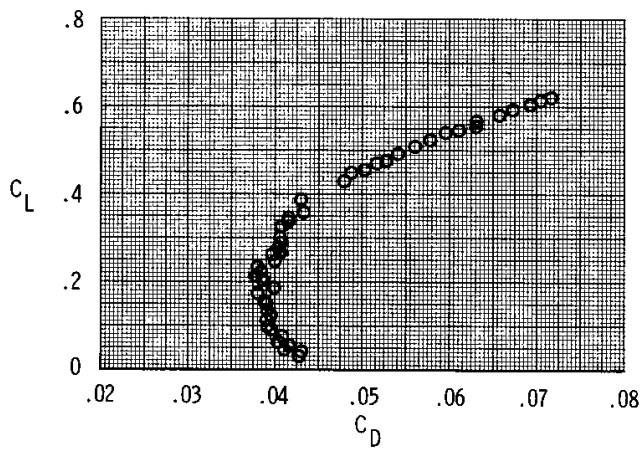

(f) $M = 0.99$, $R = 1.0 \times 10^7$.

Figure 9. Continued.

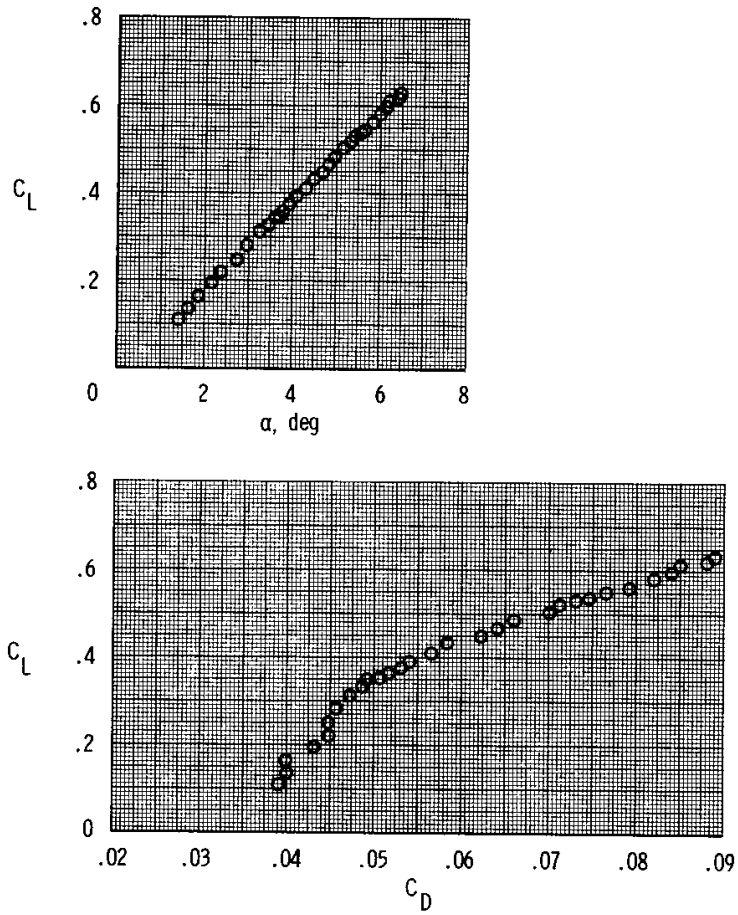

(g) $M = 1.0$, $R = 1.0 \times 10^7$.

Figure 9. Continued.

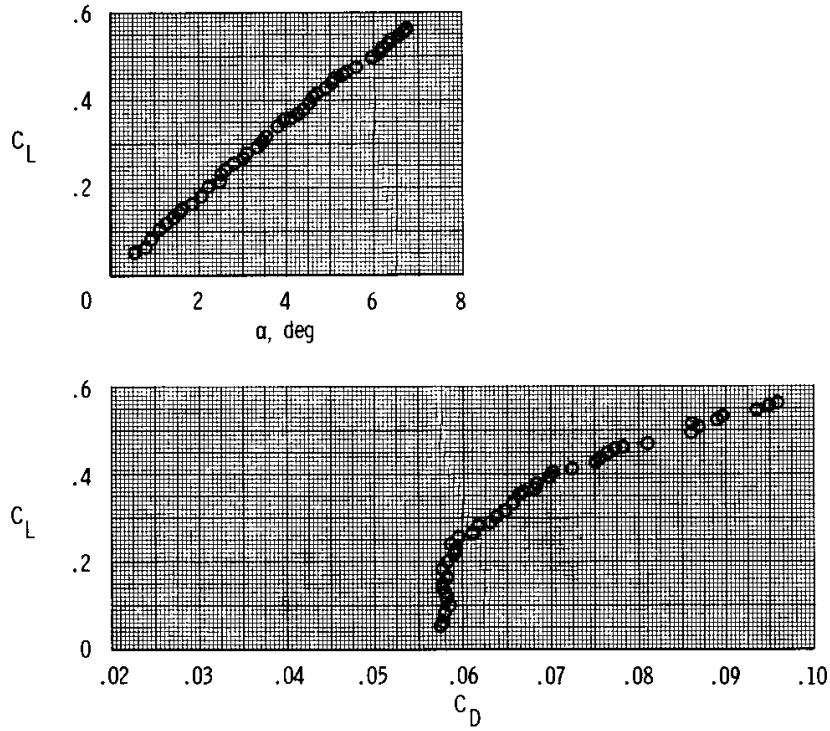

(h) $M = 1.1$, $R = 1.1 \times 10^7$.

Figure 9. Continued.

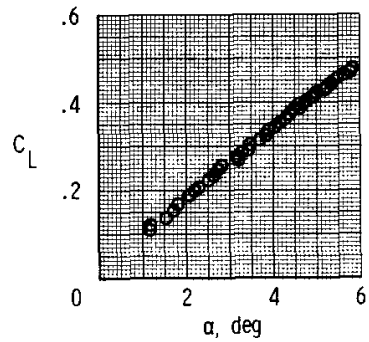

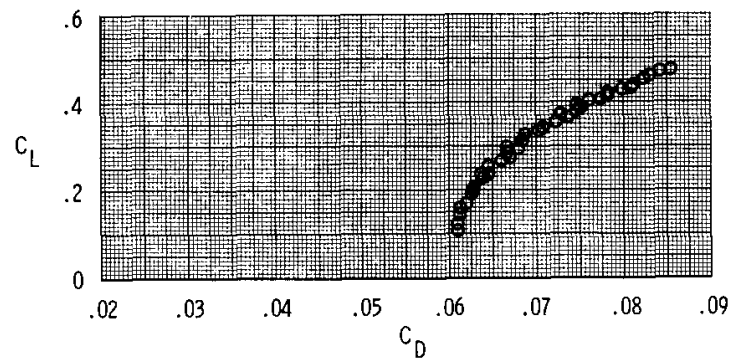

(i) $M = 1.16$, $R = 1.2 \times 10^7$.

Figure 9. Continued.

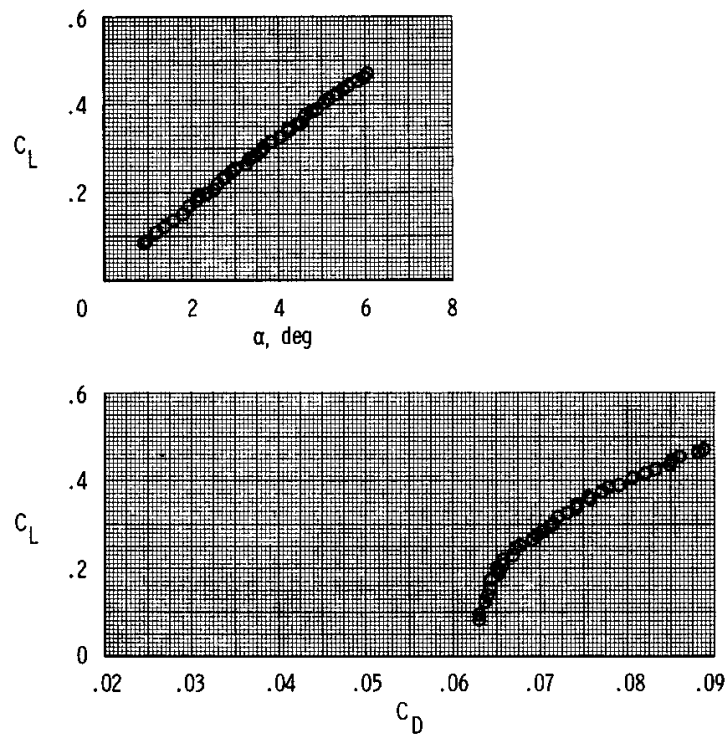

(j) $M = 1.22$, $R = 1.2 \times 10^7$.

Figure 9. Concluded.

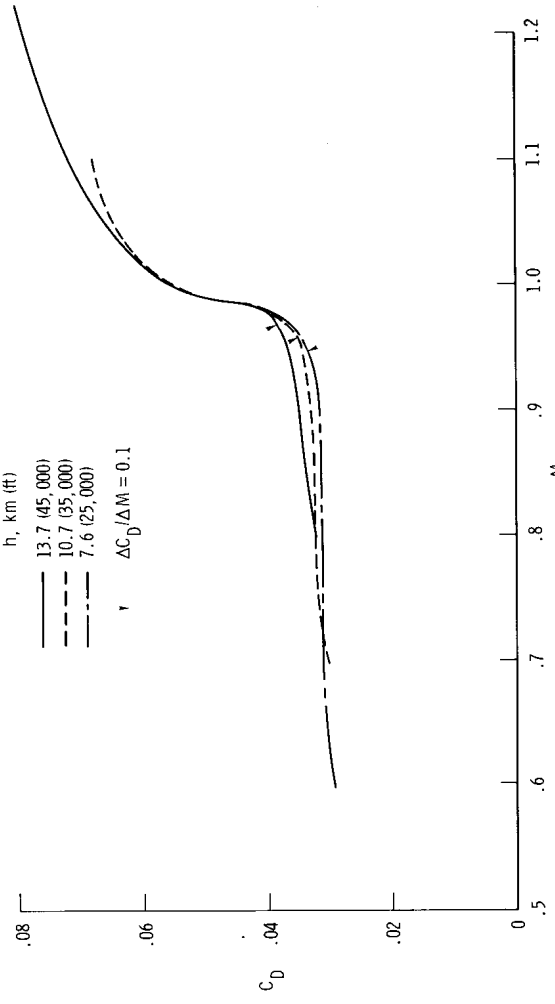

Figure 10. Variation of airplane drag coefficient with Mach number at constant altitudes. $C_L = 0.4$.

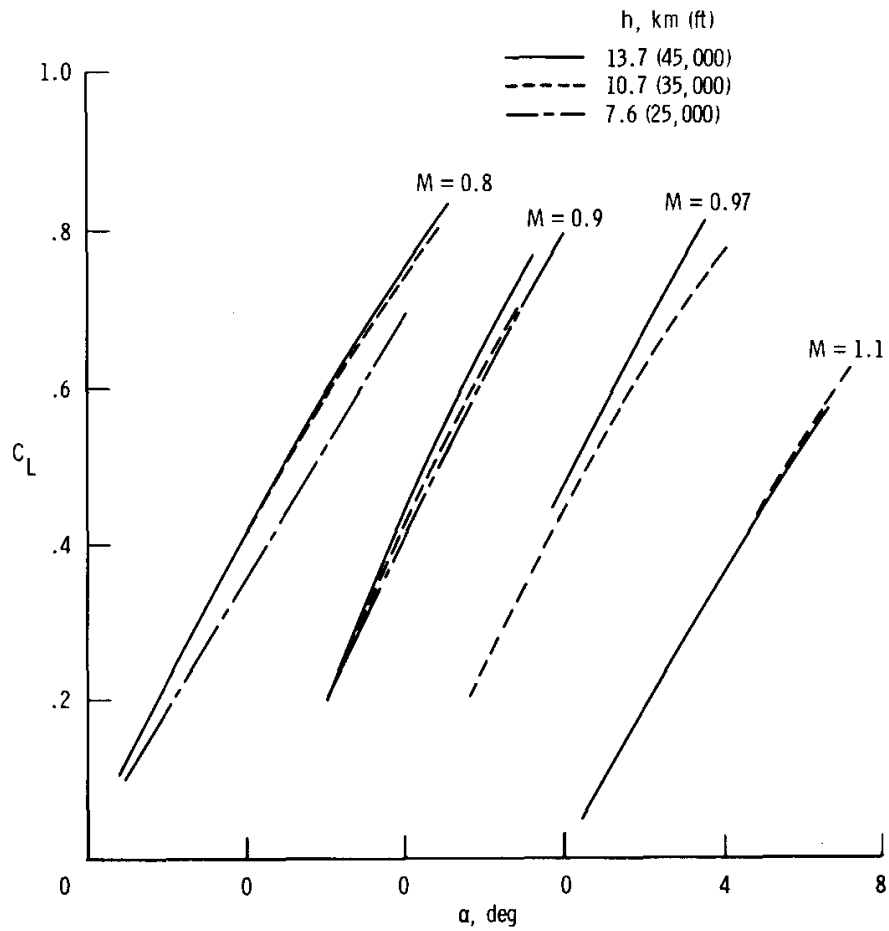

Figure 11. Effect of altitude on lift curves obtained from flight data. $R = 0.82 \times 10^7$ to 2.3×10^7.

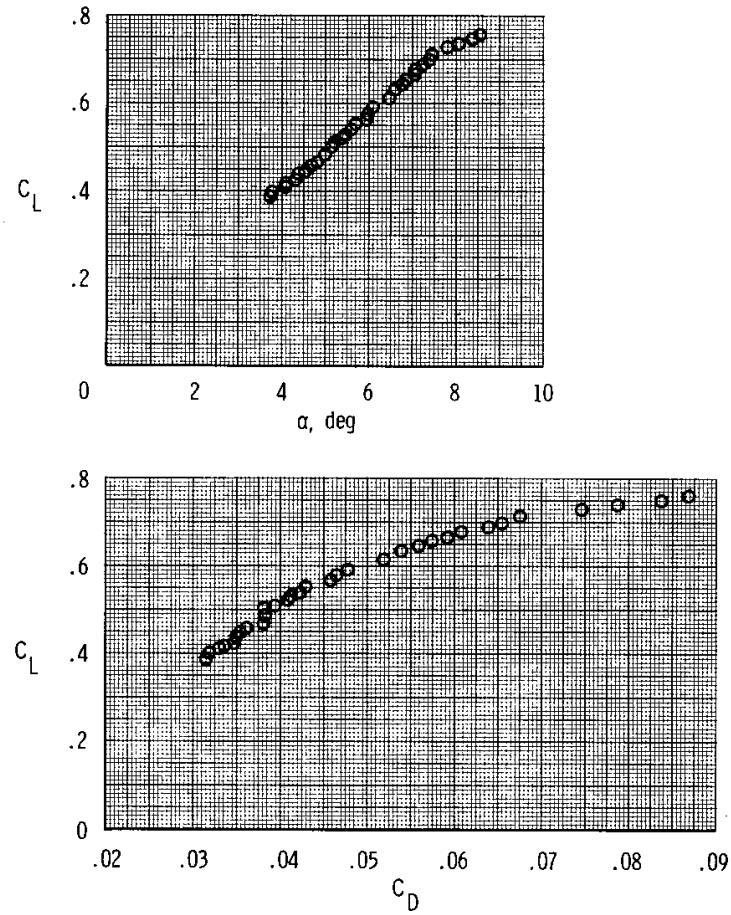

(a) $M = 0.8$, $R = 1.3 \times 10^7$.

Figure 12. Lift and drag characteristics of airplane modified with area-rule fuselage fairings. h = 10.7 kilometers (35,000 feet).

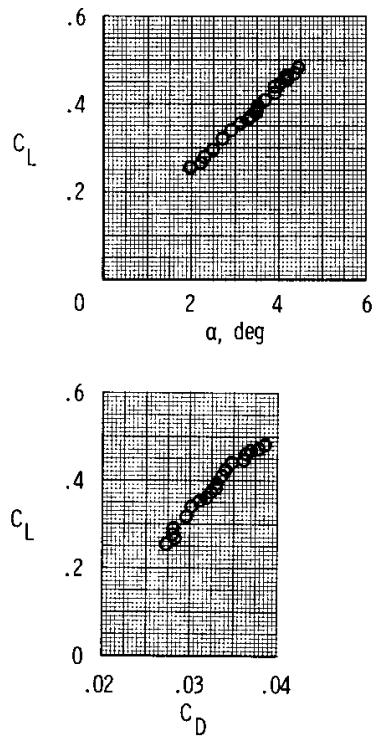

(b) $M = 0.9$, $R = 1.4 \times 10^7$.

Figure 12. Continued.

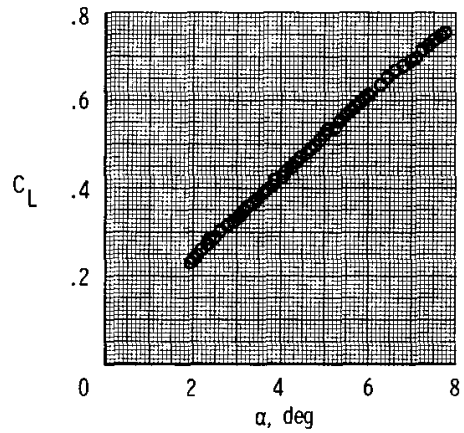

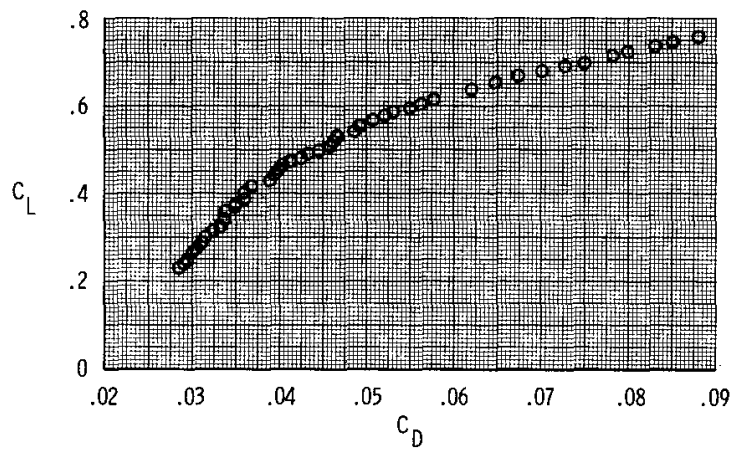

(c) $M = 0.95$, $R = 1.5 \times 10^7$.

Figure 12. Continued.

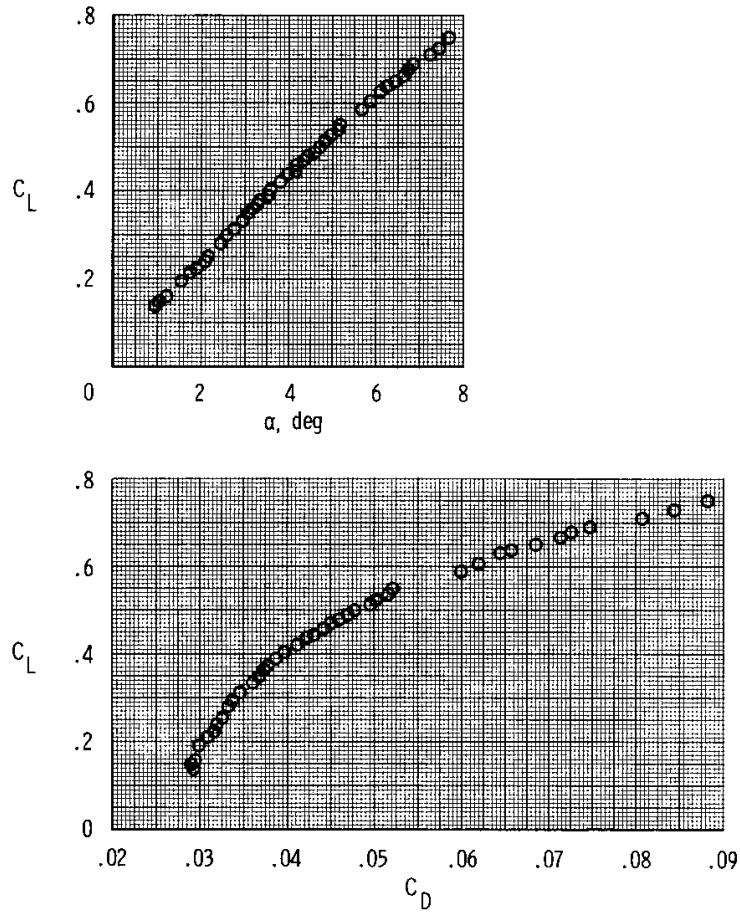

(d) $M = 0.97$, $R = 1.5 \times 10^7$.

Figure 12. Continued.

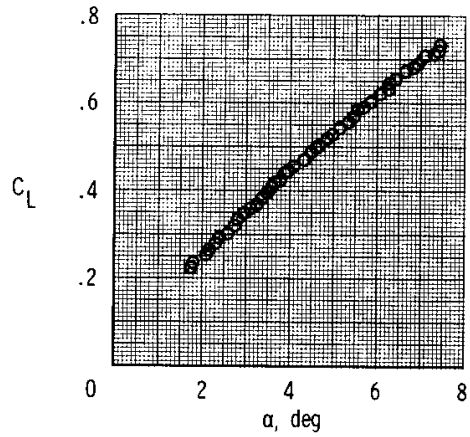

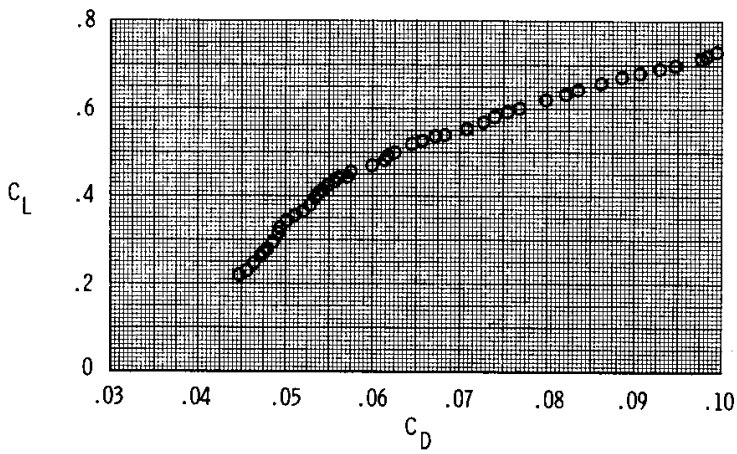

(e) $M = 0.99$, $R = 1.6 \times 10^7$.

Figure 12. Continued.

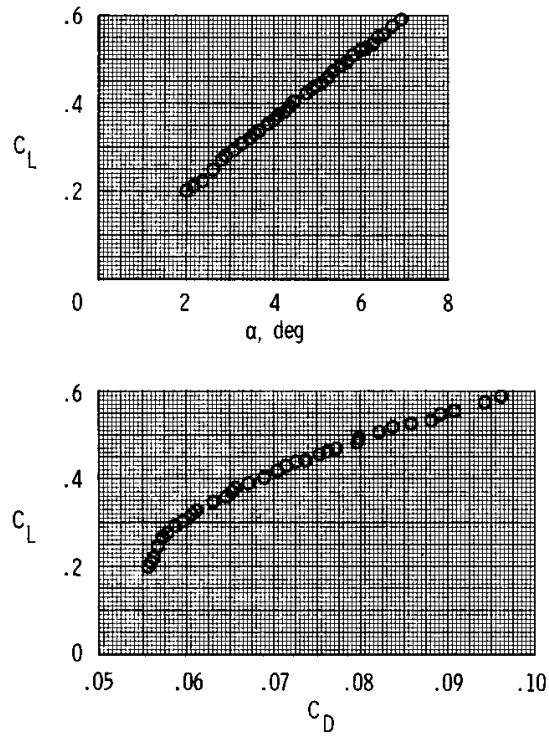

(f) $M = 1.1$, $R = 1.7 \times 10^7$.

Figure 12. Continued.

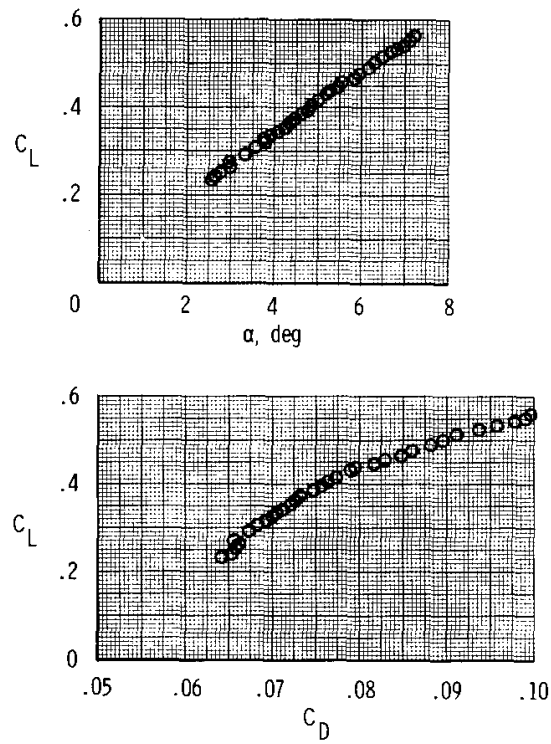

(g) $M = 1.15$, $R = 1.8 \times 10^7$.

Figure 12. Concluded.

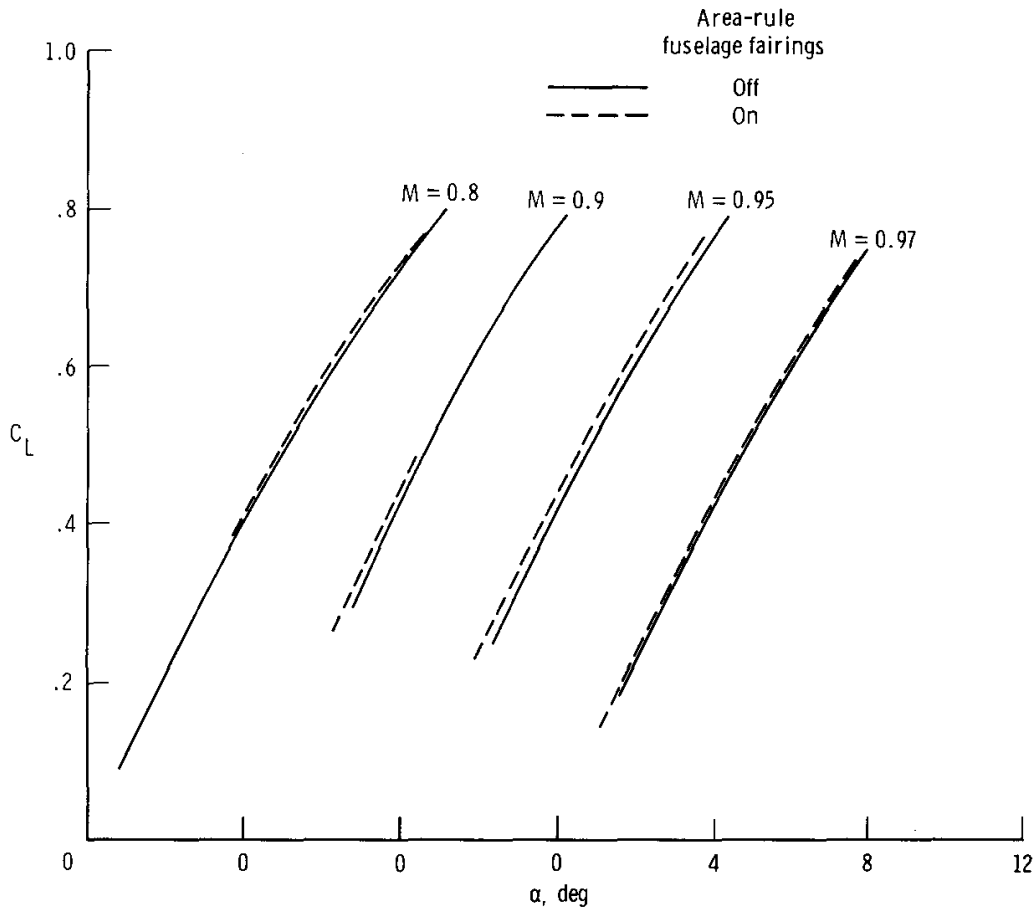

(a) Lift curves.

Figure 13. Effect of area-rule fuselage fairings on airplane lift and drag characteristics. h = 10.7 kilometers (35,000 feet).

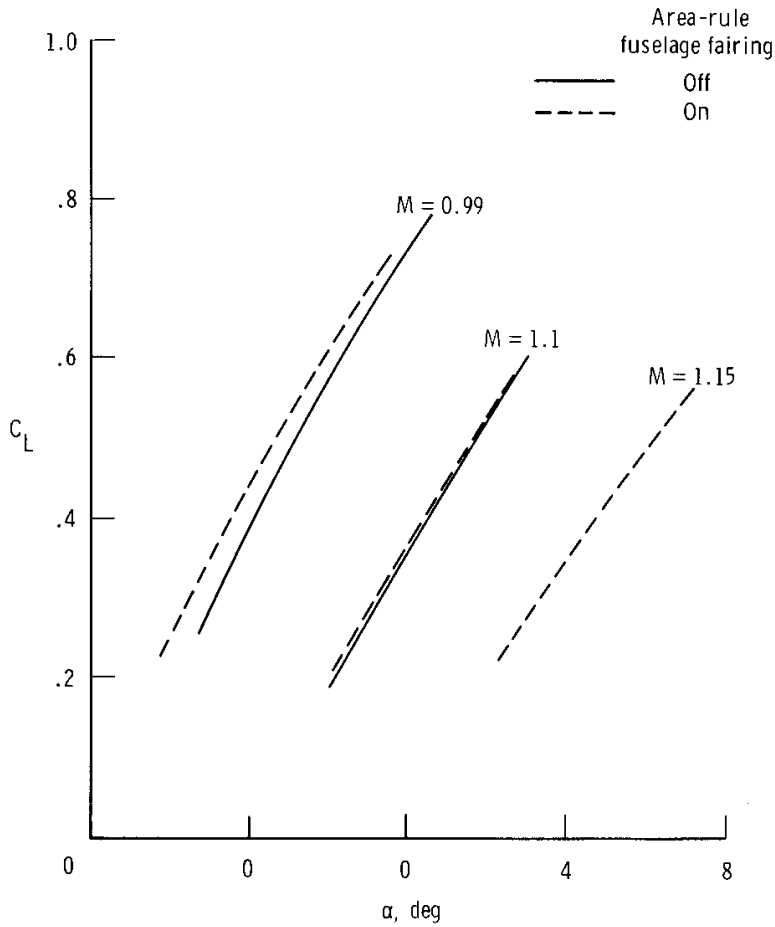

(a) Concluded.

Figure 13. Continued.

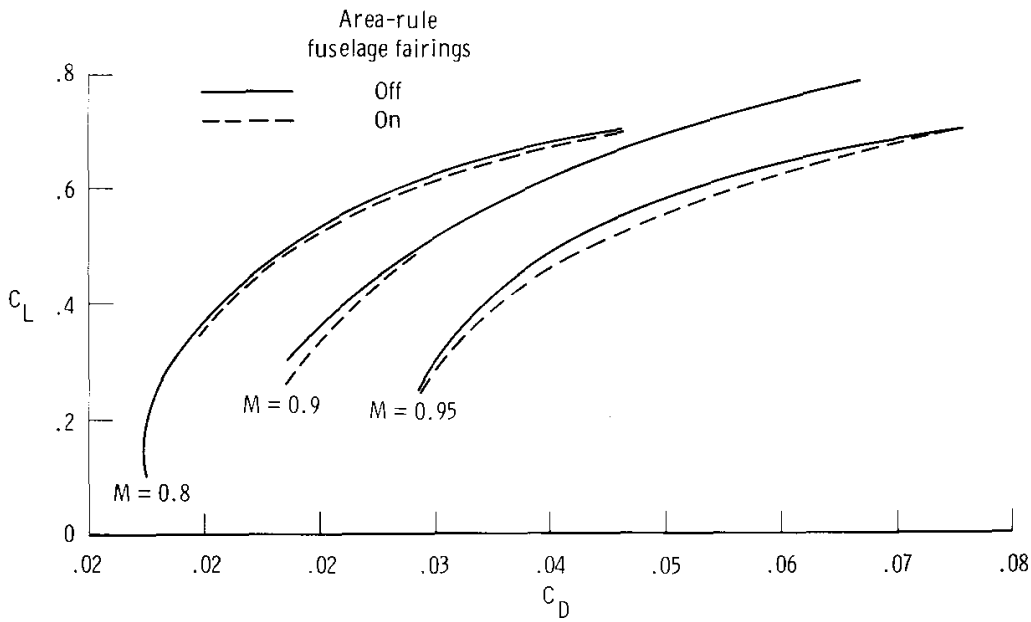

(b) Drag polars.

Figure 13. Continued.

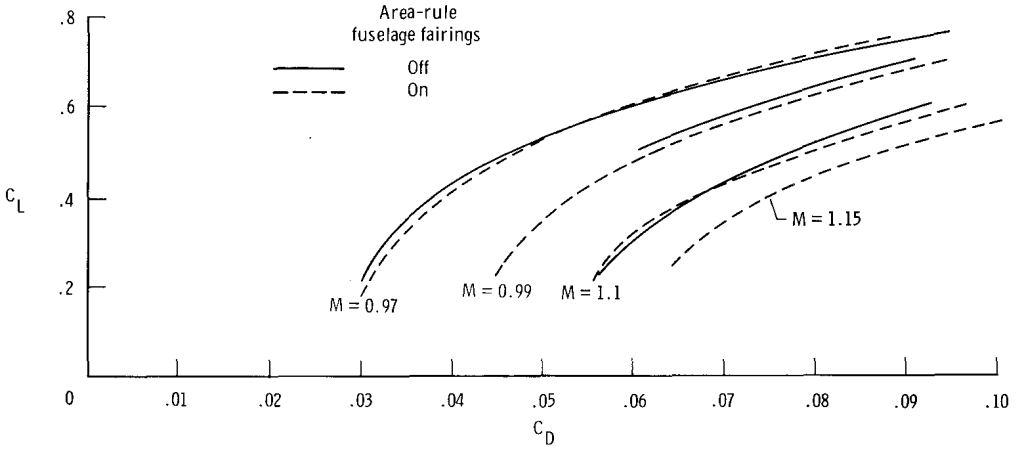

(b) Concluded.

Figure 13. Concluded.

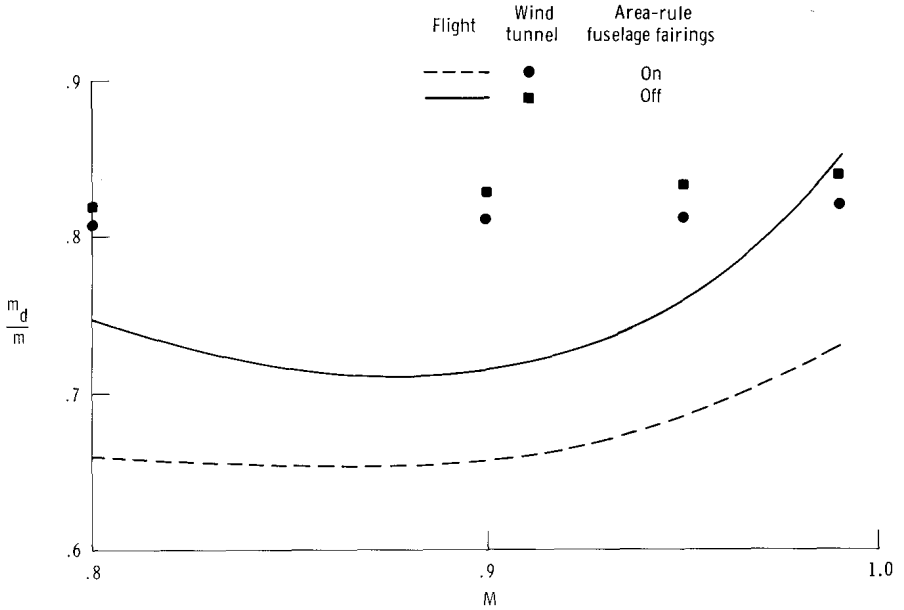

Figure 14. Mass flow ratios of airplane and wind-tunnel model with and without area-rule fuselage fairings. α = 4°.

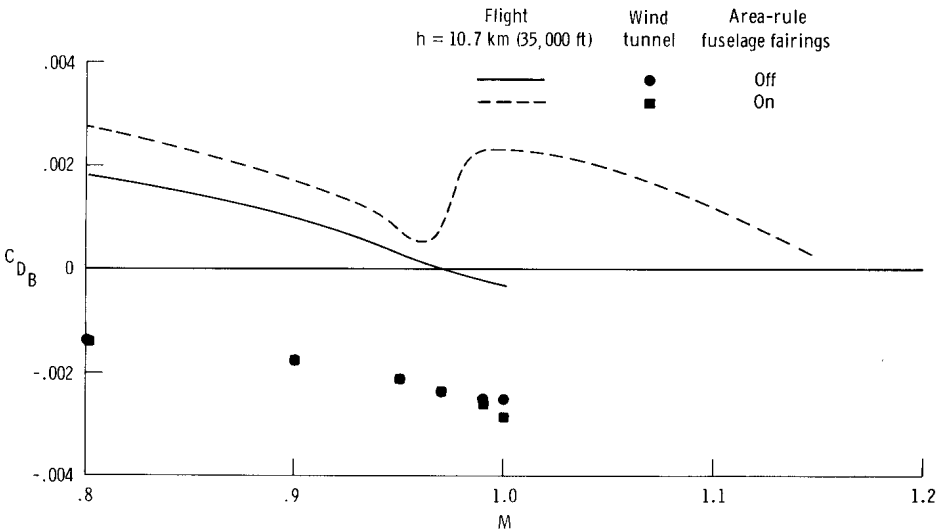

Figure 15. Comparison of base drag measured on airplane and wind-tunnel model with and without area-rule fuselage fairings. $C_L = 0.4$.

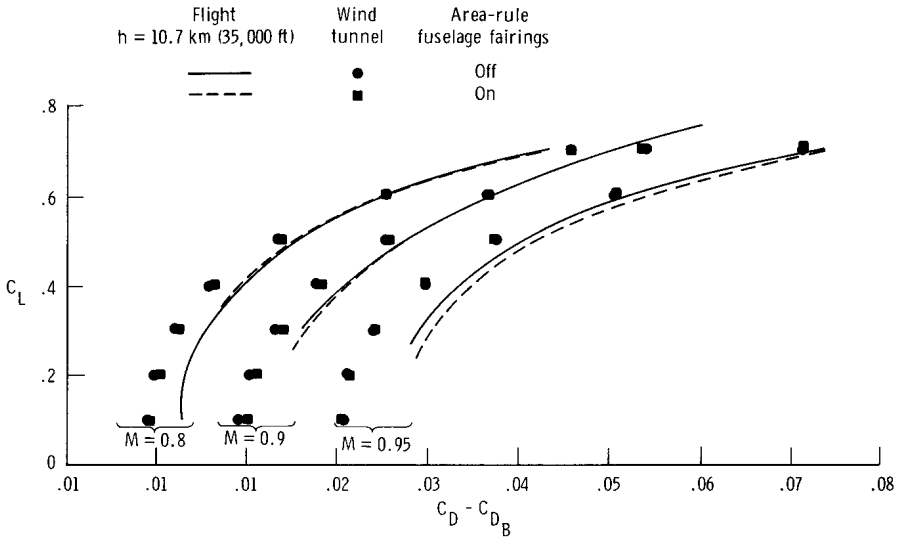

Figure 16. Comparison of flight and wind-tunnel drag polars. Base drag is subtracted from both flight and wind-tunnel results.

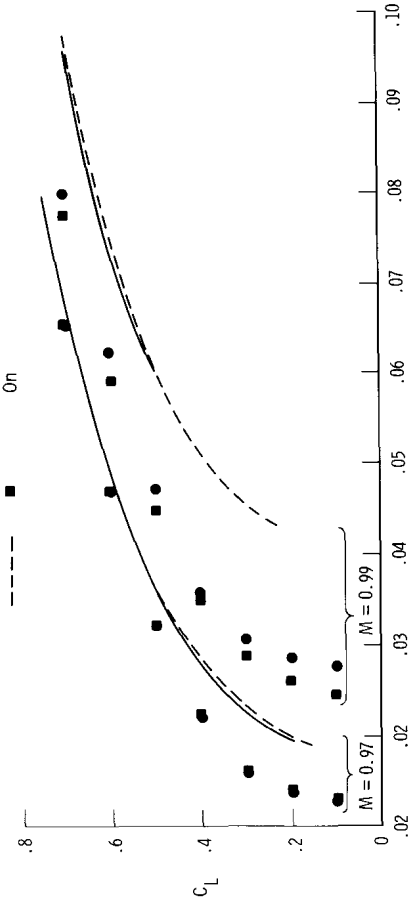

Figure 16. Concluded.

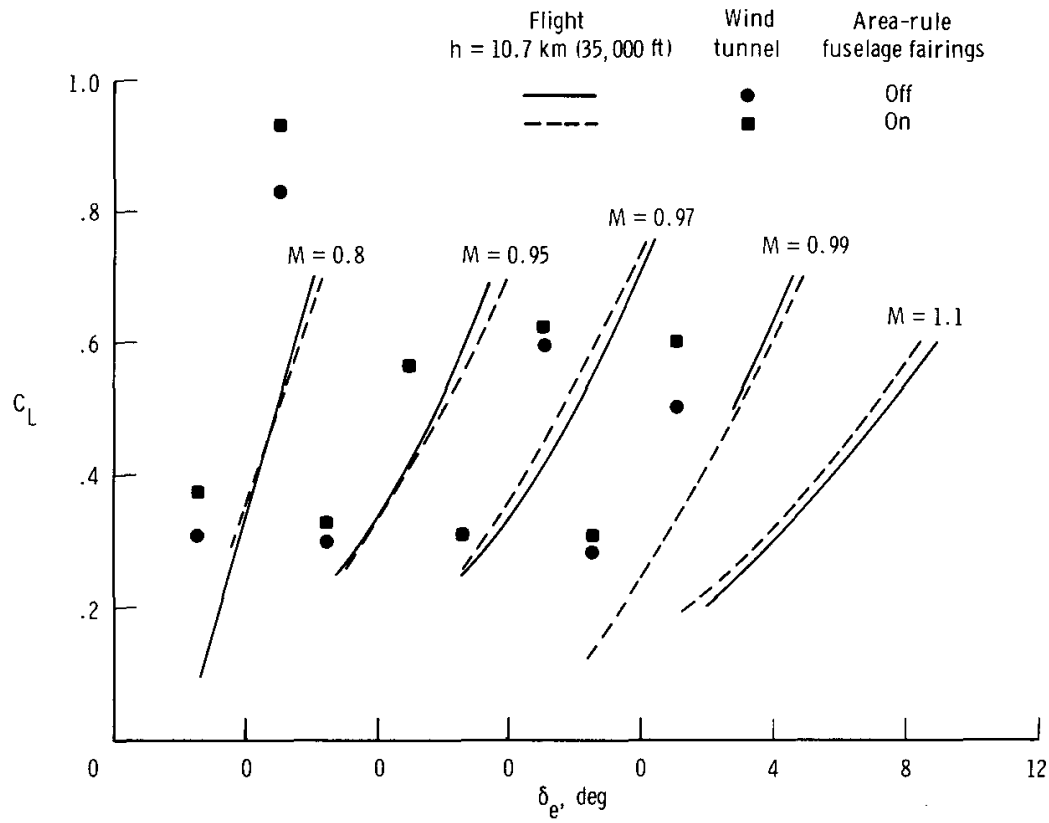

Figure 17. Comparison of flight and wind-tunnel horizontal stabilizer deflections.

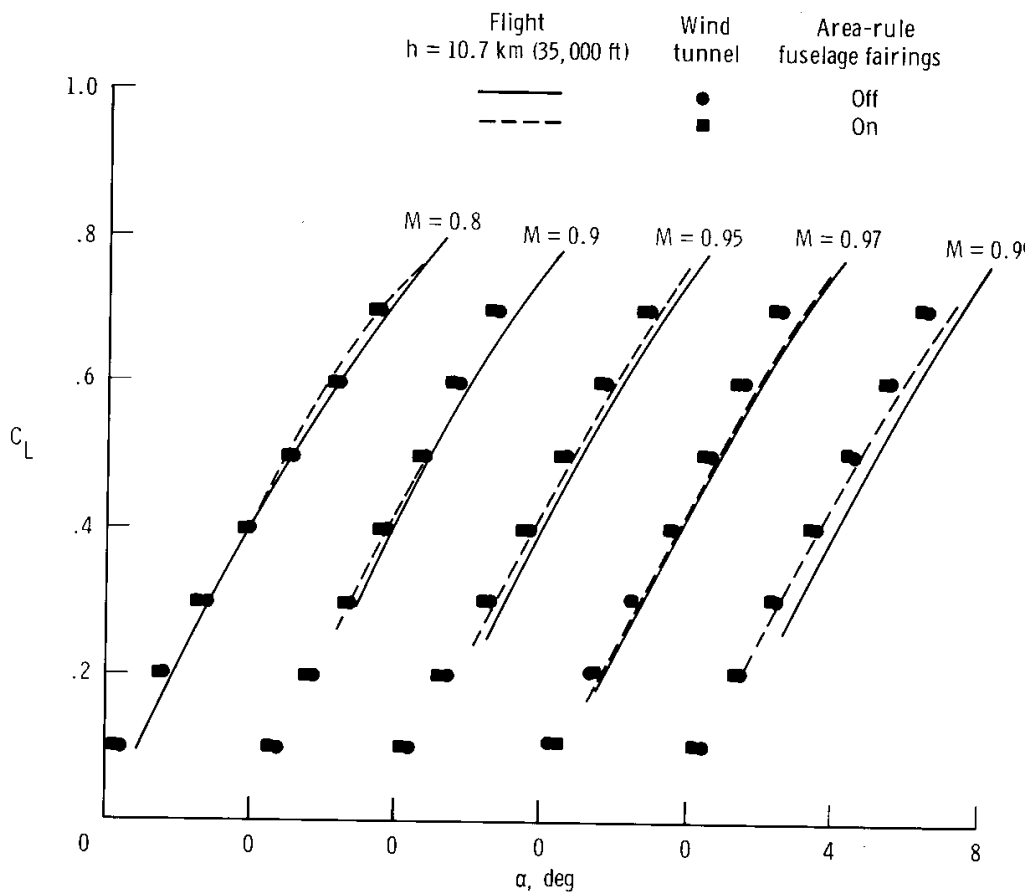

Figure 18. Flight and wind-tunnel lift curves with and without area-rule fuselage fairings.

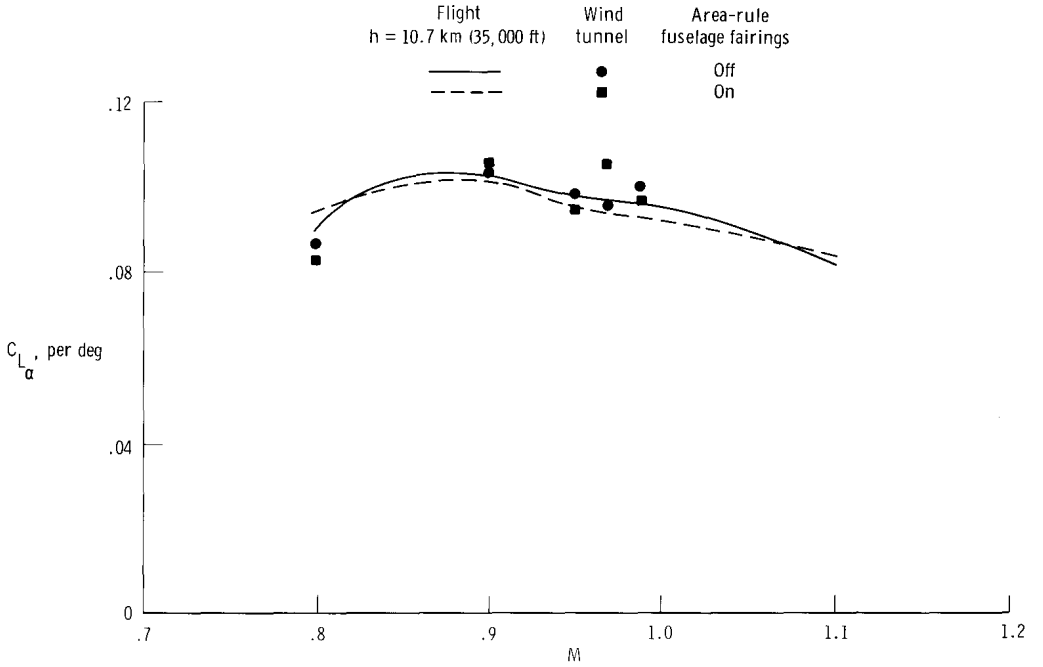

Figure 19. Comparison of lift-curve slopes obtained from airplane and wind-tunnel model with and without area-rule fuselage fairings. $C_L = 0.4$.

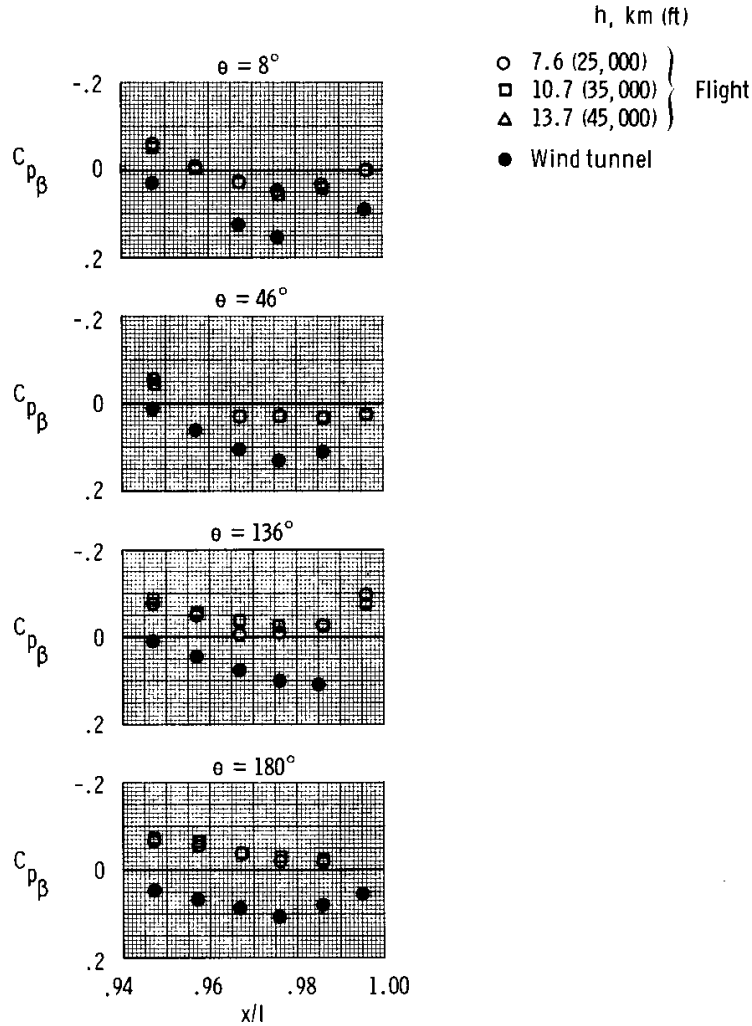

(a) With area-rule fuselage fairings.

Figure 20. Boattail pressure coefficient measured on aft fuselage shroud of airplane and wind-tunnel model with and without area-rule fuselage fairings. M = 0.9.

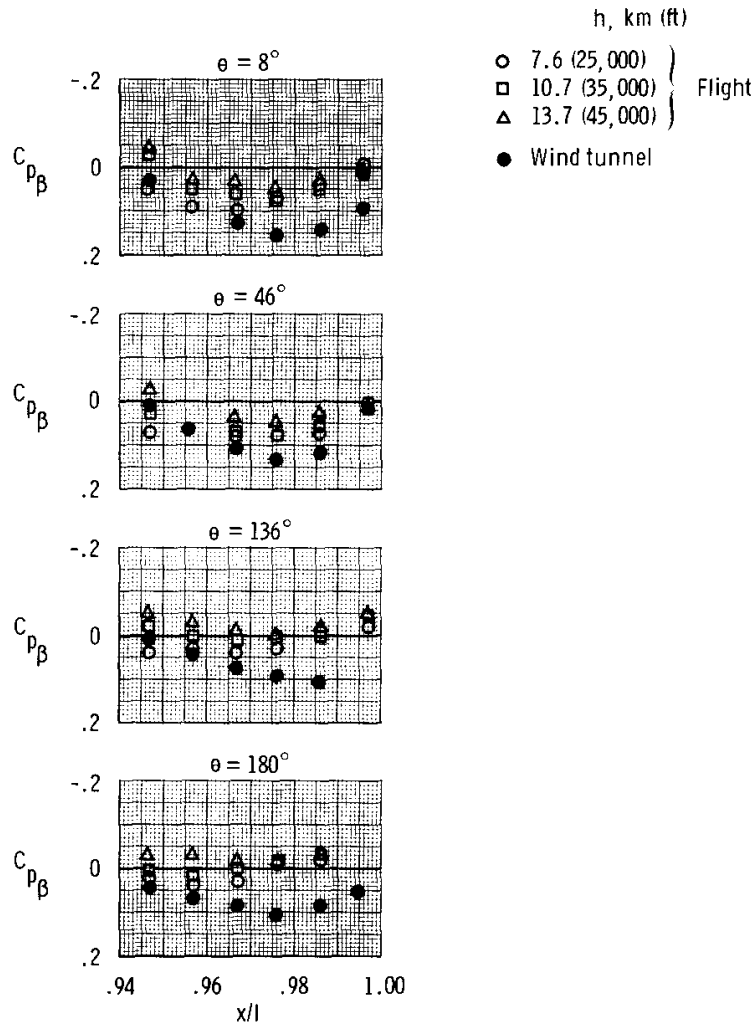

(b) Without area-rule fuselage fairings.

Figure 20. Concluded.

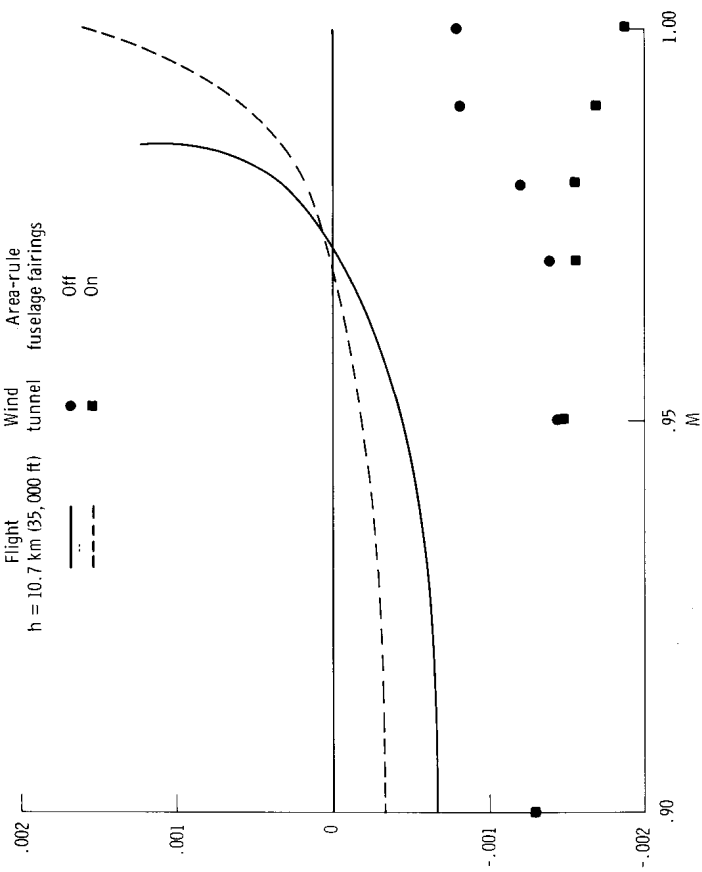

Figure 21. Comparison of boattail drag measured on aft fuselage shroud of airplane and wind-tunnel model with and without area-rule fuselage fairings. $C_L = 0.4$.

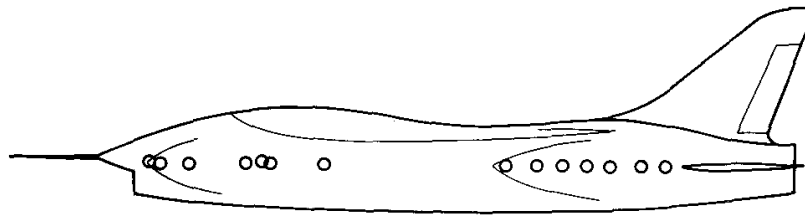

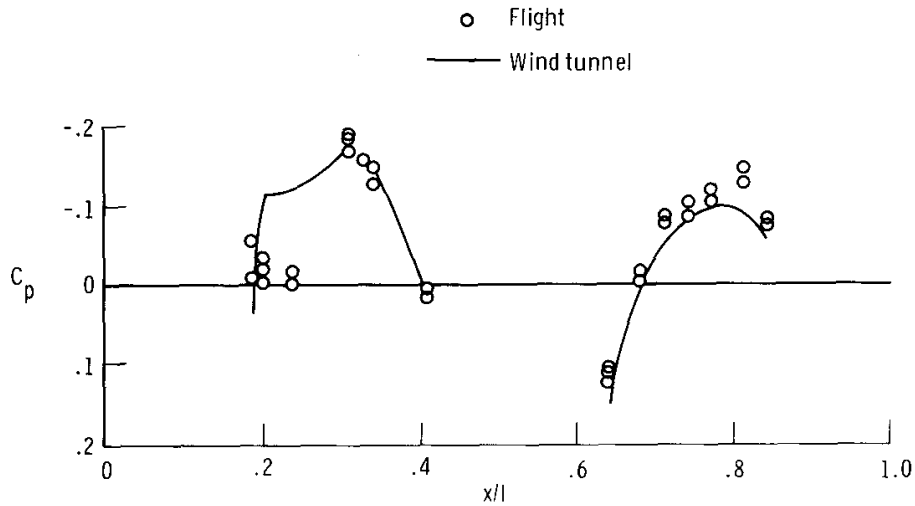

(a) M = 0.8, α = 3.3°.

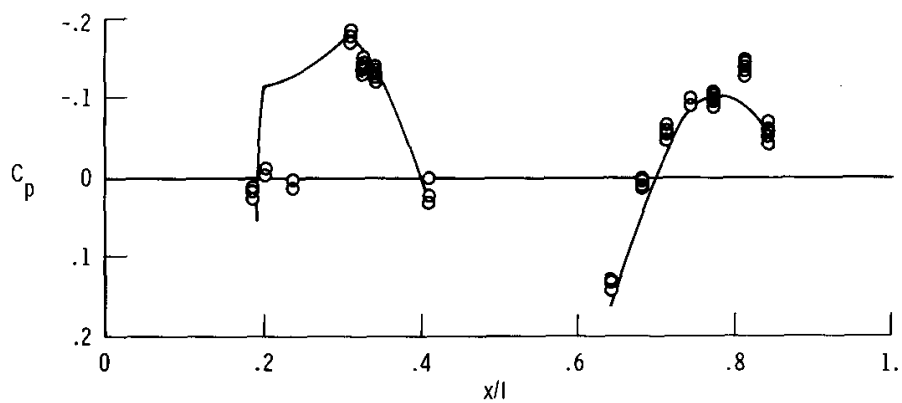

(b) M = 0.9, α = 3.1°.

Figure 22. Surface-pressure measurements along centerline of area-rule fuselage fairings from wind-tunnel model and flight tests at C_L = 0.4.

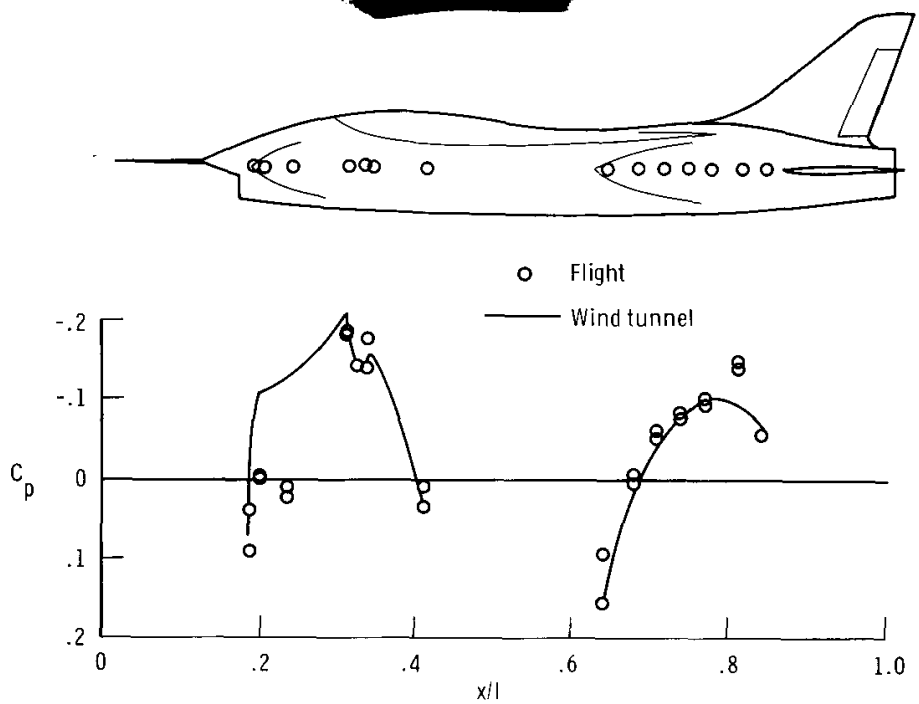

(c) $M = 0.95$, $\alpha = 3.2°$.

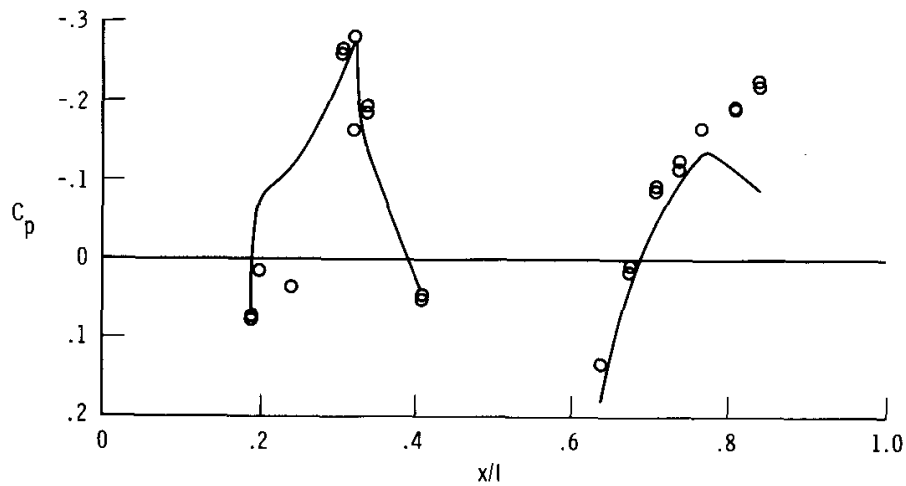

(d) $M = 0.98$, $\alpha = 3.2°$.

Figure 22. Concluded.

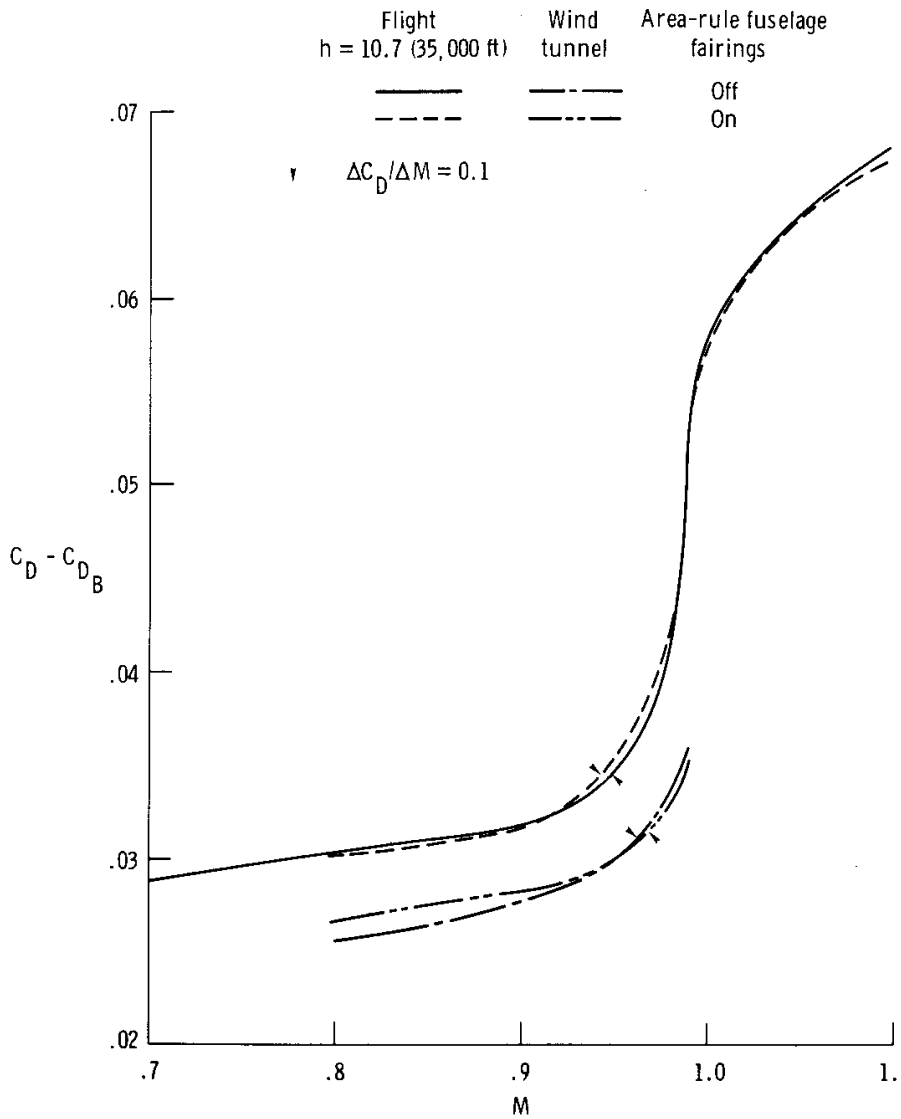

Figure 23. Variation of drag coefficient with Mach number for airplane and wind-tunnel model with and without area-rule fuselage fairings. $C_L = 0.4$.

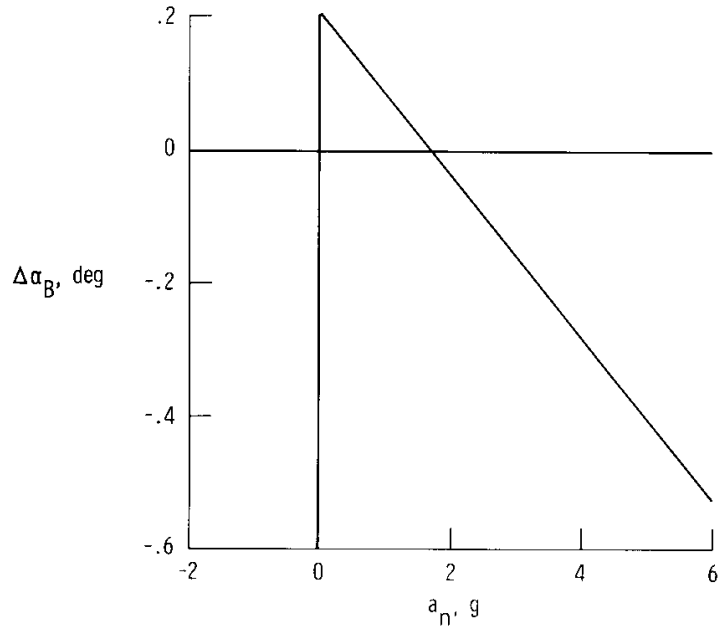

(a) Nose-boom bending correction.

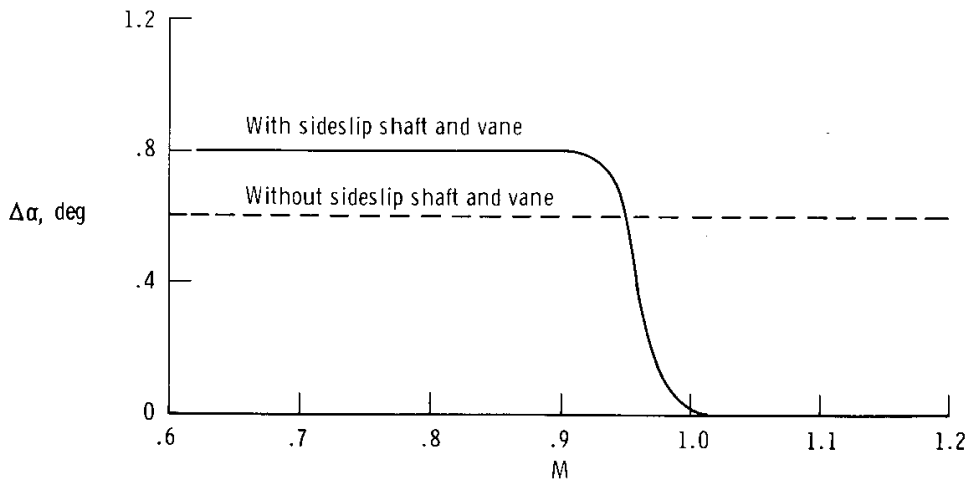

(b) In-flight angle-of-attack calibration.

Figure 24. Angle-of-attack calibrations applied to flight results.

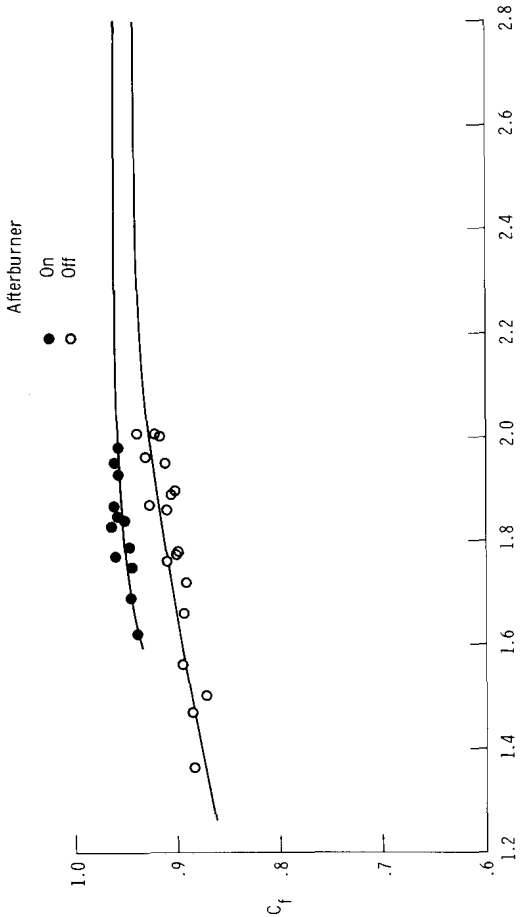

Figure 25. Extrapolation of thrust coefficients from ground thrust stand calibrations.

"The aeronautical and space activities of the United States shall be conducted so as to contribute . . . to the expansion of human knowledge of phenomena in the atmosphere and space. The Administration shall provide for the widest practicable and appropriate dissemination of information concerning its activities and the results thereof."

—NATIONAL AERONAUTICS AND SPACE ACT OF 1958

NASA SCIENTIFIC AND TECHNICAL PUBLICATIONS

TECHNICAL REPORTS: Scientific and technical information considered important, complete, and a lasting contribution to existing knowledge.

TECHNICAL NOTES: Information less broad in scope but nevertheless of importance as a contribution to existing knowledge.

TECHNICAL MEMORANDUMS: Information receiving limited distribution because of preliminary data, security classification, or other reasons.

CONTRACTOR REPORTS: Scientific and technical information generated under a NASA contract or grant and considered an important contribution to existing knowledge.

TECHNICAL TRANSLATIONS: Information published in a foreign language considered to merit NASA distribution in English.

SPECIAL PUBLICATIONS: Information derived from or of value to NASA activities. Publications include conference proceedings, monographs, data compilations, handbooks, sourcebooks, and special bibliographies.

TECHNOLOGY UTILIZATION PUBLICATIONS: Information on technology used by NASA that may be of particular interest in commercial and other non-aerospace applications. Publications include Tech Briefs, Technology Utilization Reports and Notes, and Technology Surveys.

Details on the availability of these publications may be obtained from:

SCIENTIFIC AND TECHNICAL INFORMATION OFFICE

NATIONAL AERONAUTICS AND SPACE ADMINISTRATION

Washington, D.C. 20546